ISSN 0869-5911, Petrology, 2008, Vol. 16, No. 6, pp. 584–612. © Pleiades Publishing, Ltd., 2008.
Original Russian Text © V.A. Glebovitsky, I.S. Sedova, D.I. Matukov, N.G. Berezhnaya, E.V. Tolmacheva, L.M. Samorukova, 2008, published in Petrologiya, 2008, Vol. 16, No. 6, pp. 627–656.

Geochemistry and Geochronology of Migmatites of the Kurul'ta-Nyukzha Segment and the Problem of Correlation between Metamorphic Events in the Dzhugdzhur–Stanovoi Folded Area, Eastern Siberia

V. A. Glebovitsky[a], I. S. Sedova[a], D. I. Matukov[b], N. G. Berezhnaya[b], E. V. Tolmacheva[b], and L. M. Samorukova[a]

[a] *Institute of Precambrian Geology and Geochronology (IGGD), Russian Academy of Sciences, nab. Makarova 2, St. Petersburg, 199034 Russia*
e-mail: vg@vg1404.spb.edu

[b] *Karpinskii All-Russia Research Institute of Geology (VSEGEI), Srednii pr. 74, St. Petersburg, 199106 Russia*
e-mail: sergeev@mail.wplus.net

Received November 6, 2006; in final from, December 10, 2007

Abstract—Crystalline schists of the El'gakan unit (Nyukzha River) were affected by penetrative (volume) replacement by plagiogneisses and granite-gneisses (Lc_1) and were then transformed into a polymigmatite complex with successively developing leucosomes Lc_2, Lc_3, and Lc_4. After a thrust–nappe structure was formed in response to collision processes, a new generation of granite veins was produced (Lc_5), and then tonalite gneisses Lc_6^{avt} and branching migmatites with leucosomes Lc_6^{all} were formed along strike-slip fault zones. Zircons from granite-gneisses Lc_1 were classified into four types (populations) based on SHRIMP II data. Type I (rhythmically zonal cores) were dated at 2960 and 3010 Ma, which is correlated with the age of the magmatic (predominantly volcanic) protolith. Types II and III were dated at 2703 Ma, which corresponds to granitization under amphibolite-facies conditions and the origin of the Stanoi granite-gneiss. This event is correlated with granulite metamorphism and ultrametamorphism over the whole territory of the Dzhugdzhur–Stanovoi folded area. The most widely spread type IV of the zircons has an age of 1915 Ma, which corresponds to the metamorphism coeval with overthrusting and, hence, with the collision of the Stanovoi plate and a margin of the Siberian Platform. Concentrations of REE, U, and Th and the Th/U ratio were determined to systematically decrease from type I to IV of the zircons (except their type III, whose Th/U ratio increases to >1). Zircons from Lc_5 have a concordant age of 139 Ma, which is comparable with the age of the Late Stanovoi granites. The compositional changes from the older cores to younger rims of zircons from Lc_5 are analogous to those mentioned above for zircon from Lc_1. The concordant age of zircons from Lc_6^{avt} is 127–130 Ma. Their Th/U ratio increases from cores (<1) to rims (>1), which suggests that melt may have appeared when Lc_6^{avt} was formed. ICP-MS analyses of 53 rock samples reveal differences in the character of the trend (increase/decrease) and magnitude of the changes in the concentrations of trace elements in the distinguished granitization and migmatization series; correlations were revealed between the concentrations of elements and composition of the rock groups. For example, the development of Lc_1 was associated with enrichment in Rb, Sr, Ba, LREE, Th, Zr, and Hf at depletion in Nb, Ta, U, and HREE relative to the original rocks. The leucosomes of the Lc_2, Lc_3, and Lc_4 migmatites are depleted in all of these elements except LILE, which is thought to be explained by infiltration-controlled granitization with volume replacement and partial melting at the development of vein leucosome and the subsequent mobilization of the melts together with residues. The different signs of the changes in the LREE and LILE concentrations is unusual for anatectic processes and can be modeled by equilibrium or disequilibrium melting.

DOI: 10.1134/S0869591108060040

INTRODUCTION

The genesis and age of the Stanovoi Complex in the Dzhugdzhur–Stanovoi foldbelt in southern Siberia has been studied for more than half a century. After fundamental studies conducted by D.S. Korzhinskii (1939), who distinguished the Trans-Siberian Sayan–Stanovoi Belt of supposedly Proterozoic age, all available regional geological materials were generalized and the aforementioned large regional structure was distinguished (Sudovikov et al., 1965). Simultaneously the Fore-Stanovoi Belt was distinguished as a transitional zone between the Aldan granulite area and the

Dzhugdzhur–Stanovoi foldbelt itself. All supracrustal and plutonic rocks were grouped into three complexes: Paleoarchean Aldan, Neoarchean Stanovoi, and Paleoproterozoic Dzheltulak. Intrusive rocks of various composition with the predominance of granitoids were subdivided into numerous complexes, and their ages were correlated (based on geological features) with those of supracrustal sequences. This subdivision of the rock associations survived until nowadays, although isotopic age data and recently obtained isotopic geochemical lines of evidence have notably modified the concepts of the geochronology of this region, its geological evolutionary history, and geodynamic environments. This pertains, first and foremost, to the granitoids, many of which were thought to be Early Precambrian (Sudovikov et al., 1965) but were eventually proved to be Mesozoic (Larin et al., 2000a, 2000b, 2001). This was determined not only for the allochthonous granitoids but also for large parauchtochtonous massifs that were previously included in the Late Stanovoi and Tukuringra complexes. Unfortunately, geochronological information on the Stanovoi gneiss unit, which is widespread in the Dzhugdzhur–Stanovoi foldbelt is very scarce, although it is of paramount importance for understanding the nature and evolution of this territory. The age of the Stanovoi unit can be constrained by dating the Stanovoi (Old Stanovoi) granites, which occur mostly as autochthonous bodies. Following Korzhinskii (1939) and Sudovikov et al. (1965), the latter were interpreted as produced by the migmatization of gneiss sequences.

Our research was centered on the analysis of available data on the petrology and geochemistry of the Stanovoi Complex, which is represented by the El'gakan unit in our study area (gneisses and crystalline schists of the amphibolite facies, migmatites developing after these rocks, and autochthonous and parautochthonous granitoids), and the correlation of granitization and migmatization under amphibolite-facies conditions with metamorphic and magmatic processes in neighboring blocks of the Dzhugdzhur–Stanovoi foldbelt. We studied the western (Kurul'ta–Nyukzha) segment of this territory (Fig. 1) and utilized materials collected along the Baikal–Amur Railroad, in the right-hand side of the Srednyaya Larba and Nyukzha rivers (Sedova and Glebovitsky, 1985), where granulites of the Larba, Nyukzha, and Kurul'ta blocks are exposed, along with amphibolite-facies gneisses of the El'gakan unit (Moskovchenko et al., 1985), which is correlated with the Stanovoi unit.

GEOLOGY

We studied the El'gakan unit, which consists, judging from the composition of the protoliths of the Stanovoi granite-gneiss and migmatites, of an association of mafic and intermediate crystalline schists and amphibolite. This composition of this group is notably different from that of the predominantly gneiss Ilikan unit, which occurs in the central part of the Dzhugdzhur–Stanovoi Foldbelt. The El'gakan unit also contains minor garnet–biotite (sometimes with sillimanite) gneisses.

The rocks of the El'gakan unit and the Larba and Nyukzha granulites and related magmatic rocks were affected by a number of deformation, metamorphic, and ultrametamorphic events, which were previously provisionally attributed to the Neoarchean and Paleoproterozoic tectono-magmatic cycles (Table 1). Prior to the events related to the El'gakan unit, the rocks of the Nyukzha blocks were affected by metamorphism and deformations of the granulite facies, which were ascribed to tectono-metamorphic cycle I, and the aforementioned younger events were combined into cycles II and III (Sedova and Glebovistky, 1985; Table 2). The key event in the succession of processes distinguished in the El'gakan unit was the thrusting of nappes, which are stacks of isoclinal folds and shear zones in between, which lie in nearly horizontally in the part of the vertical section exposed in the upper reaches of the Nyukzha River. These were predated by at least three populations of folds (F_1–F_3), which were recognized based on relations between planar and linear structural elements of the rocks and relations between the generation of migmatite leucosomes and granite-gneisses that developed after rocks of the El'gakan unit. The further evolution was related to the overprint of folding onto the nappes (IID_5 and IID_6), when the modern northwest-trending structure that stretches along the western riverside of the Nyukzha was formed. Cycle III was masked by the formation of a new thrust–nappe structure ($IIID_1$: N_1 and S_1) and, then, granitization (Lc_6^{avt}) and partial melting (Lc_6^{all}). It is important to mention that all of the endogenic processes recognized in the area were separated in time by the development of imbricated nappe systems.

METAMORPHISM

Information on the metamorphic conditions of the Larba Complex can be found in (Kastrykina, 1983; Shul'diner et al., 1983; Moskovchenko et al., 1993). The high Mg mole fraction of the garnet (which contains 42% of the pyrope end member) in its assemblages with biotite and sillimanite or with orthopyroxene and biotite suggests that the temperature of the metamorphic culmination was higher than 850°C (Shul'diner et al., 1983). Inasmuch as the gneisses are affected by strong diaphthoresis, their metamorphic conditions were evaluated using the TWEEQU method and the compositions of the homogeneous cores of garnet, orthopyroxene, and plagioclase grains. These conditions were proved close to equilibrium ones: T = 830°C and P = 9.5 kbar. Similar values (T = 860°C and P = 10 kbar) were obtained for associations of clinopyroxene and orthopyroxene, garnet, plagioclase, and quartz in the mafic rocks. Note that the zircon that

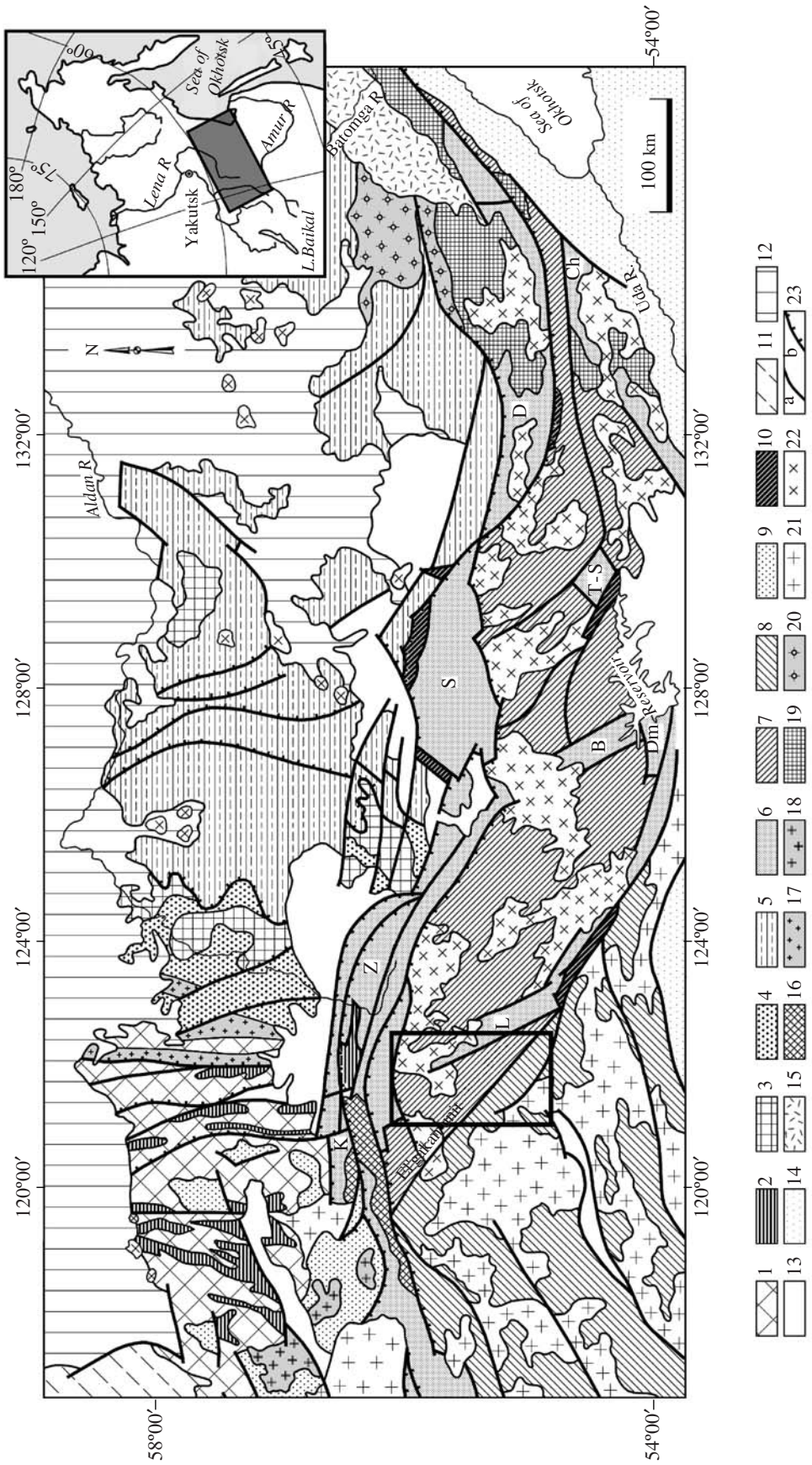
Sea of Okhotsk
Batomga R
Ch
Udal R
100 km
N
Aldan R
D
S
T-S
B
Dm
Z
K
L
Yakutsk
Lena R
Amur R
L.Baikal
180°
120°
150°
60°
75°
132°00′
128°00′
124°00′
120°00′
58°00′
54°00′

Fig. 1. Schematic tectonic map of the Aldan Shield and Dzhugdzhur–Stanovoi foldbelt (prepared by A.M. Larin).
(1, 2) Olekma Neoarchean granite–greenstone terrane: (1) tonalite–trondhjemite–gneiss complex, (2) greenstone complex; (3) most ancient Paleoarchean blocks of the Aldan granulite–gneiss terrane; (4) high-grade metamorphic complexes of the Iengra type (aluminous gneisses and schists, quartzites); (5) Early Proterozoic supracrustal complexes of the Aldan granulite–gneiss terrane; (6) allochthons of lower and mid-crustal mafic granulites, enderbites, and charnockites in the Dzhugdzhur–Stanovoi foldbelt and Stanovoi suture zone (B—Bryantinskii, Ch—Chogar, D—Dzhugdzhur, Dm—Dambukta, K—Kurul'ta and Kalar, L—Larba, S—Sutam, T-S—Tok–Sivakan, Z—Zverev); (7) Stanovoi Complex; (8) Early Proterozoic supracrustal complexes of the Selenga–Stanovoi superterrane; (9) metasedimentary complexes in depressions of the Udokan type; (10) rift grabens (troughs of the Dzheltulak type); (11) supracrustal complexes of the Patom Highland; (12) platform cover of the Siberian craton; (13) Jurassic deposits; (14) folded structures of the Central Aldan belt; (15) Okhotsk–Chukotka volcanic belt, rifts, and overprinted depressions; (16) Kalar massif of massif-type (autonomous) anorthosites (anorthosites, gabbroids, jotunites, and charnockites dated at 2.63 Ga); (17) Neoarchean granitoids; (18) Paleoproterozoic postcollision granitoids of the Kalar Complex (1.88–1.87 Ga); (19) Dzhugdzhur Massif of massif-type anorthosites (anorthosites, gabbroids, jotunites, and monzonites dated at 1.74 Ga); (20) Ulkan volcanoplutonic complex (rapakivi, alkali granites, and related bimodal volcanic rocks dated at 1.73–1.70 Ga), layered mafite–ultramafite plutons of various age; (21, 22) Phanerozoic granitoids and alkali rocks of (21) the Selenga–Stanovoi superterrane and (22) Dzhugdzhur–Stanovoi foldbelt; (23) (a) faults and (b) overthrusts.

yielded an age of 2650 ± 20 Ma (Bibikova et al., 1984) was obtained from exactly these rocks, in which it occurred as inclusions in three garnet grains.

The bulk of the El'gakan unit of the Stanovoi Complex is metamorphosed in our territory to the high-temperature amphibolite facies of elevated pressures (kyanite–sillimanite facies series) and is regionally migmatized. The examined vertical section of the El'gakan unit composes nappes and is overlain by granulite-facies rocks of the Larba block. At the same time, metamorphism of Stanovoi time is known to display some

Table 1. Succession of geological events in rocks of the El'gakan unit during tectono-metamorphic cycles II and III

Deformation stages	Structural features	Magmatism and ultrametamoprhism	Structural relations
Cycle II: amphibolite facies			
		Metamorphosed gabbroids	
IID_1	F_1, isoclinal; S_1 along AP	Lc_1: *Bt* and *Bt–Hbl* plagiogranite-gneisses and granite-gneisses	Along AP of F_1
		Diorite, granodiorite, and granite dikes	
IID_2	F_2 isoclinal; S_2 along AP	Lc_2: leucocratic *Bt* plagiogranites and granites	Along AP of F_2
IID_3	F_3 small, in shear zones; Fr_3	Lc_3: *Bt* (sometimes with *Hbl*) tonalites, plagiogranites, and granites	Along Fr_3
IID_4	F_4 isoclinal; S_4 along AP; nappes	Lc_4: *Bt* granites (often with *Grt*), *Kfs* porphyroblasts	Along AP of F_4
IID_5 and IID_6	F_5 and F_6 open and isoclinal	Lc_5: *Bt* granites correlated with the Late Stanovoi granites	Along AP of F_5 and F_6
Cycle III: amphibolite facies			
$IIID_1$	N_1; F_1; S_1	Metamorphosed gabbro, diorites, granodiorites, and granites (dikes)	Along N_1 and S_1 in the AP of F_1
$IIID_2$, $IIID_3$, $IIID_4$	F_2, F_3, and F_4 open folds and flexures related to shear zones	Lc_6^{avt}: autochthonous *Bt–Hbl* and *Bt* tonalites and granodiorites grading into allochthonous varieties during Lc_6^{all} mobilization; Lc_7–*Bt* granites	Along shear zones, AP of F_2, S, faults

Note: Roman numerals at D denote cycle numbers, F_1–F_6 are successive populations (generations) of folds, S_1–S_4 are generations of crystallization schistosity, N is overthrusts, AP is the axial planes of folds, Fr are shear zones, Lc_1 are plagiogranites and granite-gneisses, Lc_2–Lc_7 are successive populations (generations) of migmatite leucosomes.

Table 2. Isotopic data on zircons from granite-gneisses Lc_1 (sample 1515d/1)

Spot	Zircon type	Concentration						Age, Ma		Disc, %	Isotopic ratios								
		$^{206}Pb_c$, %	U, ppm	Th, ppm	Th/U	$^{232}Th/^{238}U$	$^{206}Pb^*$, ppm	$^{206}Pb/^{238}U$	$^{207}Pb/^{206}Pb$		$^{238}U/^{206}Pb^*$	±, %	$^{207}Pb^*/^{206}Pb^*$	±, %	$^{207}Pb^*/^{235}U$	σ, %	$^{206}Pb^*/^{238}U$	±, %	Err corr
1.1	II	0.06	437	22	0.05	0.05	166	2364 ± 12	2712 ± 18	15	2.256	0.62	0.1866	1.10	11.40	1.20	0.4431	0.62	0.507
2.1	III	0.00	29	63	2.17	2.21	13.2	2703 ± 27	2650 ± 16	–2	1.920	1.20	0.1796	0.95	12.90	1.60	0.5209	1.20	0.790
3.1	I	0.01	846	194	0.23	0.24	366	2629 ± 12	2912 ± 4	11	1.986	0.54	0.2108	0.24	14.64	0.59	0.5035	0.54	0.914
4.1	I	0.01	1075	517	0.48	0.50	487	2730 ± 12	2874 ± 3	5	1.896	0.52	0.2059	0.21	14.97	0.56	0.5273	0.52	0.927
4.2	IV	0.06	208	12	0.06	0.06	61.1	1897 ± 11	2173 ± 19	15	2.922	0.66	0.1357	1.10	6.40	1.30	0.3420	0.66	0.516
4.3	I	0.04	184	57	0.31	0.32	85.9	2791 ± 15	2899 ± 6	4	1.845	0.68	0.2092	0.40	15.63	0.79	0.5418	0.68	0.861
5.1	III	0.21	56	98	1.66	1.79	29.4	3054 ± 27	2725 ± 23	–11	1.647	1.10	0.1880	1.40	15.71	1.80	0.6060	1.10	0.629
6.1	II	–	2515	260	0.10	0.11	952	2354 ± 10	2688 ± 7	14	2.269	0.51	0.1839	0.40	11.18	0.65	0.4408	0.51	0.787
7.1	IV	0.69	39	2	0.05	0.04	10.3	1728 ± 18	1844 ± 42	7	3.231	1.10	0.1127	2.30	4.78	2.60	0.3074	1.20	0.454
7.2	II	0.38	752	90	0.12	0.12	245	2068 ± 10	2625 ± 6	27	2.634	0.55	0.1771	0.34	9.23	0.64	0.3783	0.55	0.852
8.1	II	–	429	37	0.09	0.09	169	2440 ± 30	2620 ± 11	7	2.174	1.50	0.1764	0.69	11.19	1.60	0.4601	1.50	0.905
9.1	IV	0.30	18	0	0	0.01	5.4	1923 ± 26	1904 ± 42	–1	2.869	1.50	0.1166	2.30	5.59	2.80	0.3476	1.50	0.551
10.1	IV	0.15	38	0	0	0.01	11.1	1876 ± 20	1903 ± 32	1	2.956	1.20	0.1165	1.80	5.43	2.10	0.3377	1.20	0.575
11.1	IV	0.06	31	0	0	0.00	9.1	1900 ± 21	1889 ± 27	–1	2.916	1.30	0.1156	1.50	5.46	2.00	0.3427	1.30	0.644
12.1	III	0.07	50	114	2.28	2.36	22.8	2743 ± 22	2706 ± 13	–1	1.884	0.98	0.1859	0.79	13.59	1.30	0.5304	0.98	0.779
13.1	IV	1.65	7	0	0	0.01	2.12	1917 ± 42	1900 ± 100	–1	2.839	2.40	0.1163	5.80	5.55	6.30	0.3464	2.50	0.397
14.1	II	0.01	845	222	0.26	0.27	347	2518 ± 11	2762 ± 6	10	2.092	0.54	0.1923	0.39	12.67	0.67	0.4779	0.54	0.807
15.1	IV	0.15	16	1	0.06	0.03	4.92	1922 ± 28	1889 ± 50	–2	2.874	1.70	0.1156	2.80	5.54	3.30	0.3474	1.70	0.517
1.1.1	I	0.06	516	111	0.22	0.22	209	2490 ± 9	2759 ± 7	10	2.1209	0.43	0.1920	0.44	12.48	0.61	0.4715	0.43	0.699
1.2.1	I	0.02	526	356	0.68	0.70	213	2486 ± 16	2857 ± 7	13	2.125	0.78	0.2039	0.44	13.23	0.90	0.4706	0.78	0.872
1.3.1	I	0.01	2307	766	0.33	0.34	1070	2784 ± 7	2923 ± 5	5	1.8510	0.32	0.2124	0.29	15.82	0.43	0.5403	0.32	0.741

Table 2. (Contd.)

Spot	Zircon type	Concentration						Age, Ma		Disc, %	Isotopic ratios								
		$^{206}Pb_c$, %	U, ppm	Th, ppm	Th/U	$^{232}Th/^{238}U$	$^{206}Pb^*$, ppm	$^{206}Pb/^{238}U$	$^{207}Pb/^{206}Pb$		$^{238}U/^{206}Pb^*$	±, %	$^{207}Pb^*/^{206}Pb^*$	±, %	$^{207}Pb^*/^{235}U$	σ, %	$^{206}Pb^*/^{238}U$	±, %	Err corr
1.4.1	I	0.02	988	204	0.21	0.21	450	2740 ± 8	2982 ± 7	8	1.8878	0.37	0.2203	0.44	16.09	0.57	0.5297	0.37	0.646
1.5.1	II	0.01	1096	18	0.02	0.02	340	1989 ± 6	2552 ± 8	22	2.767	0.38	0.1694	0.47	8.44	0.60	0.3614	0.38	0.629
1.6.1	I	0.02	379	98	0.26	0.27	190	2964 ± 13	2945 ± 7	–1	1.7128	0.54	0.2152	0.42	17.32	0.68	0.5838	0.54	0.793
1.7.1	II	0.09	370	36	0.10	0.10	123	2104 ± 11	2552 ± 11	18	2.591	0.61	0.1694	0.64	9.02	0.88	0.3859	0.61	0.689
1.6.2	I	0.01	718	239	0.33	0.34	352	2914 ± 10	3000 ± 5	3	1.7495	0.41	0.2227	0.34	17.55	0.54	0.5716	0.41	0.773
1.6.3	II	0.10	227	41	0.18	0.19	81.9	2261 ± 14	2735 ± 12	17	2.380	0.73	0.1892	0.73	10.96	1.00	0.4201	0.73	0.707
1.8.1	I	0.00	289	25	0.09	0.09	139	2858 ± 17	3017 ± 9	5	1.792	0.75	0.2251	0.58	17.32	0.94	0.5579	0.75	0.792
1.8.2	I	0.03	1031	35	0.03	0.03	404	2420 ± 7	2819 ± 5	14	2.1952	0.35	0.1991	0.32	12.51	0.48	0.4555	0.35	0.736
1.9.1	IV	0.00	431	11	0.03	0.03	120	1804 ± 7	2080 ± 11	13	3.096	0.47	0.1287	0.64	5.73	0.79	0.3230	0.47	0.586
1.9.2	III	0.04	45	97	2.16	2.20	20.5	2723 ± 29	2703 ± 22	–1	1.902	1.3	0.1856	1.40	13.45	1.90	0.5257	1.30	0.696
1.9.3	II	0.02	569	67	0.12	0.12	210	2306 ± 8	2603 ± 7	11	2.3247	0.40	0.1746	0.44	10.36	0.59	0.4302	0.40	0.673
1.10.1	I	0.00	336	145	0.43	0.45	149	2689 ± 13	2842 ± 8	5	1.932	0.57	0.2019	0.52	14.41	0.77	0.5176	0.57	0.738
1.11.1	II	0.01	1230	79	0.06	0.07	523	2594 ± 7	2741 ± 4	5	2.0184	0.31	0.1899	0.25	12.97	0.40	0.4954	0.31	0.777
1.11.2	IV	1.60	79	3	0.04	0.04	23.8	1912 ± 21	1977 ± 79	3	2.896	1.2	0.1214	4.40	5.78	4.60	0.3453	1.20	0.271
1.12.1	I	–	1584	419	0.26	0.27	730	2768 ± 5	2976 ± 7	7	1.8645	0.24	0.2194	0.47	16.23	0.52	0.5363	0.24	0.452
1.12.2	III	0.02	382	133	0.35	0.36	144	2348 ± 10	2634 ± 14	11	2.276	0.53	0.1780	0.84	10.78	0.99	0.4393	0.53	0.535
1.12.3	IV	0.00	15	0	0	0.01	4.56	1946 ± 41	1872 ± 85	–4	2.838	2.4	0.1145	4.70	5.56	5.30	0.3524	2.40	0.457
1.13.1	II	0.00	959	301	0.31	0.32	375	2417 ± 6	2742 ± 5	12	2.1981	0.30	0.1900	0.30	11.92	0.43	0.4549	0.30	0.714
1.13.2	III	0.03	61	139	2.28	2.35	27.4	2709 ± 25	2696 ± 19	–1	1.914	1.1	0.1847	1.20	13.30	1.60	0.5224	1.10	0.689
1.13.3	IV	0.25	170	10	0.06	0.06	52.6	1974 ± 21	1931 ± 21	–2	2.791	1.2	0.1183	1.20	5.85	1.70	0.3583	1.20	0.712

Note: Errors are given at an 1σ level. Pb_c and Pb* are common and radiogenic Pb, respectively. The calibration error of the standard does not exceed 0.38%. Correction for common Pb is introduced according to measured ^{204}Pb. Err corr is the correlation coefficient between the $^{207}Pb^*/^{235}U$ and $^{206}Pb^*/^{238}U$ ratios; Disc is the discordance coefficient: $100[1 - (^{206}Pb/^{238}U \text{ age})/(^{207}Pb/^{206}Pb \text{ age})]$.

zoning. In the basin of the Nyukzha River, zones corresponding to the staurolite–biotite–kyanite–muscovite, garnet–kyanite–biotite–muscovite, kyanite–biotite–garnet–orthoclase, and sillimanite–biotite–garnet–orthoclase subfacies were distinguished (Kastrykina, 1983). Conceivably, granulites of the Larba block were the high-temperature part of this zoning. Later, in the course of tectono-metamorphic cycle III, the rocks were deformed and metamorphosed to the low-temperature amphibolite–epidote-amphibolite facies. In unevenly distributed blastomylonite zones, hornblende and plagioclase are recrystallized, and more sodic newly formed plagioclase occurs, along with muscovite and epidote. The rocks are locally affected by granitization and diatexis.

GRANITIZATION AND MIGMATIZATION

We examined relations between the products of granitization and migmatization and those and magmatic rocks separating them in exposures displaying direct relations between these rock types. The earliest of the recognized event was the granitization of the El'gakan unit and the development of the Stanovoi granite-gneiss complex, which was later affected by multiple events of anatectic migmatization (Fig. 1). Because of this, the rocks of the El'gakan unit are, in fact, polymigmatites that developed after biotite and amphibole granite-gneisses and granodiorite-gneisses (Lc_1) with relics of crystalline schists and amphibolites (Fig. 2b). The earlier leucosomes (Lc_1) are sometimes oriented along the axial planes of isoclinal folds F_1 in amphibolites with beds of amphibole gneisses.[1] This setting is typical of the second-population leucosomes (Lc_2) (Figs. 2c–2e), which are veins of biotite and amphibole (sometimes with garnet) granites (Figs. 2d, 2e). These leucosomes are separated from Lc_1 by diorite, tonalite, and granite dikes (Figs. 2e, 2l). The leucosomes of the third population (Lc_3) developed along cutting zones (Fr_3) as amoeba-shaped patches in granite-gneisses and migmatites (Figs. 2c, 2f, 2g, 2i). Leucosomes Lc_4 occur as series of cutting granite veins of various thickness, with sharp contacts (Figs. 2c, 2g). Veins of banded granites (Lc_5) oriented along the axial planes of open and anticlinal folds F_5 with gently dipping hinge lines (these folds overprint the nappes) are deformed, along with all earlier structures, into upright, variably compressed folds F_6. The morphology of these granites, which are correlated with the Late Stanovoi granites, is illustrated in Figs. 2h–2k. Lc_5 are usually strongly deformed (Fig. 2i) and are sometimes multiply folded into hinge-in-hinge structures (Fig. 2k). These leucosomes consist mostly of biotite granites and only occasionally contain amphibole. Their bodies are heterogeneous and show banded structures, with the banding parallel to their contacts.

Leucosomes Lc_6^{avt} attributed to the next (third) cycle (which is provisionally dated at the Early Proterozoic) consist of biotite–amphibole granites and granodiorites and are geologically clearly separated from all older leucosomes (Table 1). Their bodies have unclear diffuse contacts and are oriented parallel to the axial planes of folds of younger populations (Fig. 2m); these bodies were predated by the emplacement of dikes of metamorphosed gabbroids, which were strongly deformed (Figs. 2n–2o), diorites, tonalites, and granites. The rocks are often penetrated by network migmatite (Fig. 2o). These granites (which underwent partial melting) were sometimes highly mobile and formed intrusive bodies of capricious geometry (Lc_6^{all}, Fig. 2p) and eruption breccias, in which fragments of all older rocks are reoriented (Fig. 2r). Granites Lc_6^{avt} and Lc_6^{all} are cut by veins of leucocratic granites Lc_7, which have sharp rectilinear contacts (Fig. 2j).

Hence, based on their geological relations, it is convenient to subdivide the rocks produced by ultrametamorphism into nebulites (Lc_1 and Lc_6^{avt}), which were produced via the volume replacement of the original rocks, migmatites conformable with the layering and leucosomes Lc_2 and Lc_4, and predominantly network migmatites Lc_3 and Lc_6^{all}. The granitoids denoted Lc_5 occur as relatively small tabular bodies and ptygmatite veins no thicker than 20 cm.

The geological relations, structural setting, and petrography of the rock groups indicate that the mechanisms that produced them were different: predominantly metasomatic at partial melting during final stages for Lc_1 and Lc_6^{avt}, anatectic for Lc_2 and Lc_4, and diatectic for Lc_3 and Lc_6^{all}. Our earlier publications (Sedova and Glebovitsky, 1984; Glebovitsky et al., 2006) present evidence that the Stanovoi granite-gneisses were produced by metasomatic granitization and subsequent melting. This interpretation is close to that proposed for the Mogocha block (Gavrikova and Zharikov, 1984) west of our study area. The process should have involved the metasomatic "preparation" of the rocks and their subsequent partial melting. The mechanisms responsible for the origin of granitic melts, including those developing after mafic rocks, are continuously discussed in the literature. It was demonstrated experimentally that such rocks can melt under amphibolite- and granulite-facies conditions and infiltration-controlled granitization (Zharikov and Khodorevskaya, 2006). The genesis of granitoids Lc_5 is less certain. These granitoids comprise anatectic bodies,

[1] Here and below, Lc_1–Lc_7 are successive generations (populations) of migmatite leucosomes (from older to younger ones). When necessary, the avt and all superscript indices are used to distinguish between autochthonous (Lc_6^{avt}) and significantly displaced (allochthonous, Lc_6^{all}) veins.

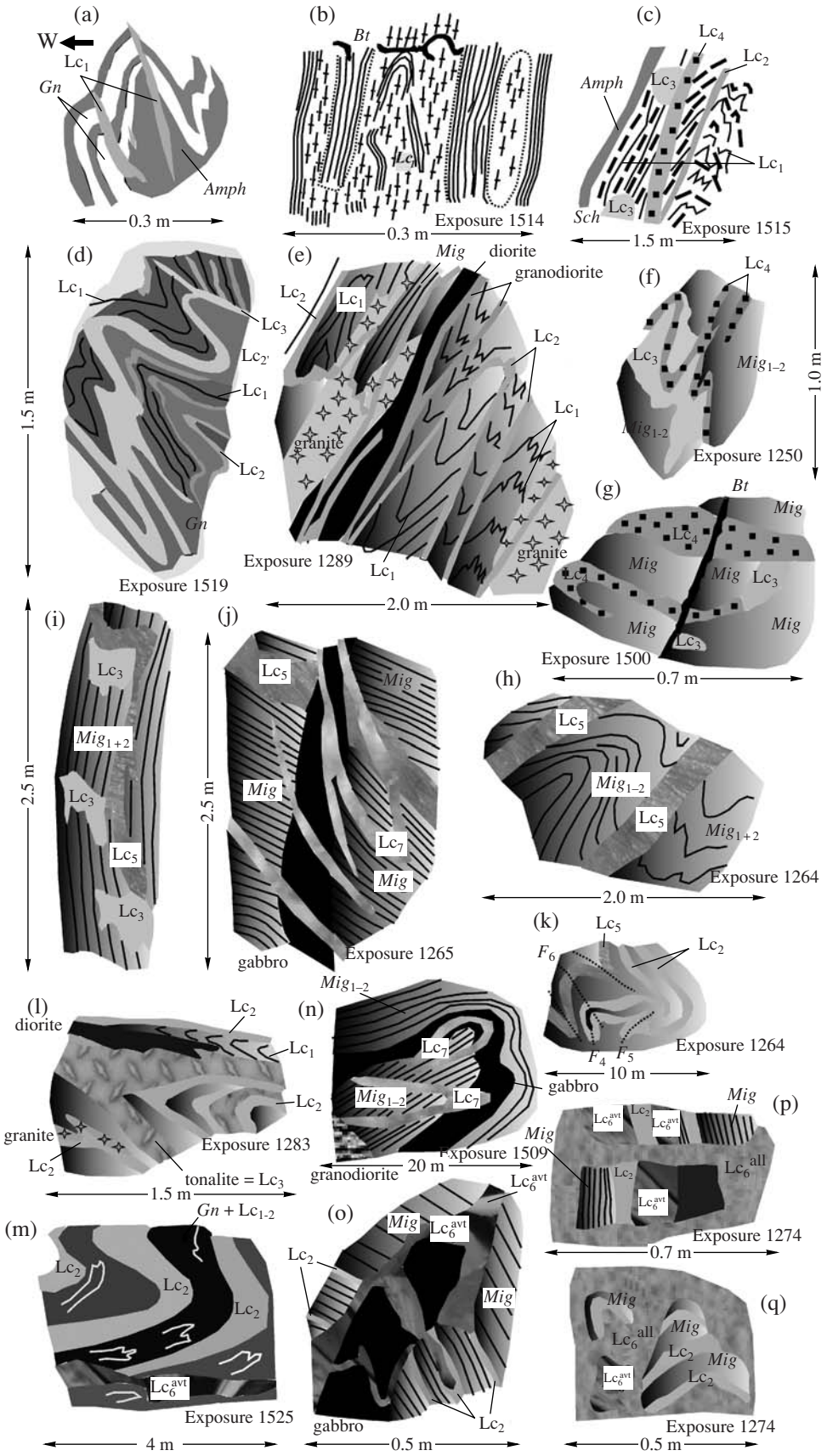

Fig. 2. Relations between plagiogneisses Lc_1 and younger populations of leucosomes in migmatites (Lc_2–Lc_7). See text for explanations. *Gn*—biotite and biotite–amphibole gneiss, *Amph*—amphibolite, *Sch*—mafic crystalline schist, *Mig*—migmatite, *Bt*—biotite.

which were produced via the partial melting of Lc_1 and are sometimes differentiated, and bodies whose melts came from deeper levels (Glebovitsky and Sedova, 1984; Sedova and Glebovitsky, 1985). Genetically similar rock groups were proved to be different not only in their age relations but also in the isotopic age.

AGE

Zircons from the rocks were dated on a sensitive high-resolution ion microprobe (SHRIMP II) at the Center for Isotopic Studies at the Karpinskii All-Russia Research Institute of Geology (VSEGEI), of the Ministry of Natural Resources of the Russian Federation. The studies were conducted on samples of Stanovoi autochthonous granite-gneisses Lc_1 (nebulites) with relict bands of biotite–amphibole crystalline schists and amphibolites (Fig. 2c, sample 1515d/1), granites from leucosome Lc_5 (Fig. 2h, sample 1264a), which were formed later than the thrust–nape structure and are correlated with the Late Stanovoi granites, and autochthonous leucosomes Lc_6^{avt} (Fig. 2p, sample 1274o).

According to their morphological and structural features and with regard for their isotopic dates and data on melt and fluid inclusions in them, zircons from granite-gneiss Lc_1 (sample 1515d/1) were classified into following four phases (genetic types, listed in order from older to younger ones):

(1) Zircons of phase I occur as pale pink thinly zonal prismatic crystals, which are surrounded by younger rims (Figs. 3a–3d). Their cores are variably preserved, and the expansion of the rims obliterates their zoning (Fig. 3e). The grains range from 150 to 250 μm, their aspect ratio (K_e) is 2–3, and their rims are from 5 to 40 μm thick. The thinly zonal cores contain 289–1096 ppm U and 23–544 ppm Th, their Th/U = 0.05–0.5 (mostly >0.2), as is typical of magmatic zircons (Varva et al., 1999). The U concentrations in the rims are 752 ppm, and their Th concentrations are 94 ppm, at Th/U = 0.12 (Table 2).

(2) Zircons of phase II are turbid brownish prismatic and rounded crystals with black metamict or weakly zonal cores and pale peripheral parts of variable thickness, which belong to younger generations (Figs. 3e–3g). The U and Th concentrations in the cores broadly vary (from 227 to 2515 and from 22 to 301 ppm, respectively), Th/U = 0.02–0.33.

(3) Zircons of phase III occur as colorless prismatic, slightly elongated or equant and rounded (Figs. 3e, 3f) grains of complicated inner structure. In cathodoluminescence (CL), it is seen that the grains include domains with traces of zoning and sectorial structures (Fig. 3e, spot 1.13.2; Fig. 3f, spot 1.9.2). The crystals are 70–400 μm, have K_e = 2–3, and contain 29–16 ppm U and 63–139 ppm Th at Th/U = 1.66–2.28, which makes this type of zircons notably different from the previous ones.

(4) Phase IV comprises the youngest, pale in CL rims of variable thickness that surround the cores of zircons I and II and rims of phase III (Figs. 3b, 3e, 3g, 3h). Sometimes they compose individual crystals and are predominant in zircon monomineralic fractions. The colorless crystals vary from 150 to 400 μm and have K_e = 2–3. Zircons of phase IV contain 7–431 ppm U, 1–10 ppm Th, and have very low Th/U ratios: 0.01–0.06. These geochemical features are typical of metamorphic zircons of the high-temperature amphibolite facies (Varna et al., 1999).

The zircon phases (types) distinguished above show clearly pronounced geochemical differences. Types I and II have similar U and Th concentrations (with the Th concentrations prone to slightly increase and defining individual correlation trends; Fig. 4). From cores (type I) to margins (type IV, Fig. 3b, spots 4.1–4.3) and from type II to type IV (Fig. 3f, spots 1.9.3–1.9.1), the Th and U concentrations tend to decrease. Type III is characterized by lower U concentrations than those in the previous two types at moderate Th concentrations, which causes a significant increase in the Th/U ratio. Type IV differs from the former two in containing lower Th and U concentrations, with the Th concentrations of some samples decreasing below the detection limit of the method. Types III and IV also sometimes define individual trends (Fig. 4).

Zircon types (phases) I–III are characterized by low positive Ce anomalies and small negative Eu anomalies (Fig. 5a). Zircons of type I differ from zircons of types II and III in having high HREE/LREE ratios. At analogous LREE concentrations, type-III zircons tend to have lower HREE concentrations than those in zircons of types I and II. Type IV displays neither Ce nor Eu anomalies and is characterized by a significant decrease in the REE concentrations (particularly those of HREE). The HREE, LREE, and Eu concentrations and the $(La/Yb)_n$ ratio generally decrease from type I to III and, particularly, type IV.

Zircons from granite Lc_5 (sample 1264a) consist of cores (likely foreign) and zonal peripheral parts (Figs. 3i–3k) and are characterized by generally much higher Th concentrations in the cores (35–1489 ppm) than in margins (0.12–0.52 ppm) at higher U concentrations (33–825 ppm in the cores and 10–130 ppm in the margins; Table 3). The Th/U ratio is higher in the cores (0.38–3.57) than margins (0.15–0.52). A systematic decrease in the U and Th concentrations and the Th/U ratio from cores to margins was revealed in a number of grains (Table 3, spots 6.1–6.2 and 7.1–7.2) but not for spots 3.2–3.1–3.1*. As in the zircons of types I and II from Lc_1 (Fig. 5b), early zircons from Lc_5 are characterized by positive Ce and negative Eu anomalies, and the later zircons are characterized by higher HREE and, particularly, LREE concentrations, and their REE patterns are similar to those of type-IV zircons from Lc_1 (their REE patterns have neither Ce nor Eu anomalies

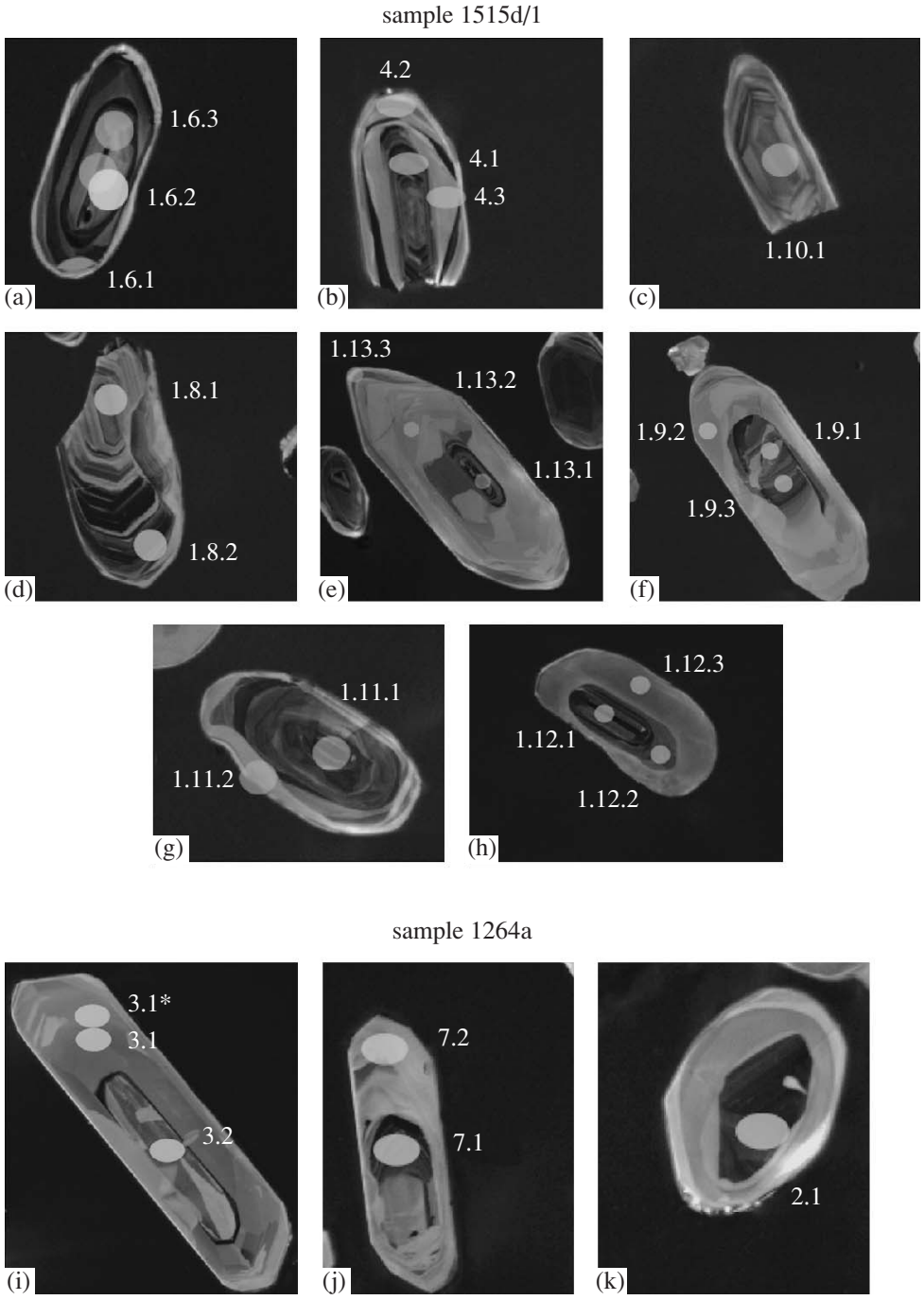

Fig. 3. Cathodoluminescence images of zircons from (a–h) plagiogranite-gneiss Lc_1 (sample 1515d/1) and (i–k) granite Lc_5 (sample 1264a). Labels (numbers) mark corresponding analytical spots.

and are characterized by lower LREE concentrations) but differ from them in having higher HREE contents.

Zircons from Lc_6^{avt} (sample 1274o) consist of cores and younger rims. The Th concentrations are 94–401 ppm in the cores and 64–1553 in the rims at similar variations in U concentrations (71–867 in the cores and 92–2233 ppm in the rims), with the Th/U ratio prone to increase from cores to rims (Table 4). Correspondingly, the zircon types are characterized by different trends (Fig. 4).

Zircon phases distinguished based on the morphology of crystals, their inner structures, geochemistry (U, Th, and REE contents) yield principally different isotopic age values, which were determined in sample 1515-d/1 (granite-gneiss Lc_1) at more than 50 spots, in sample 1264-a at 12 spots, and in sample 1274o at

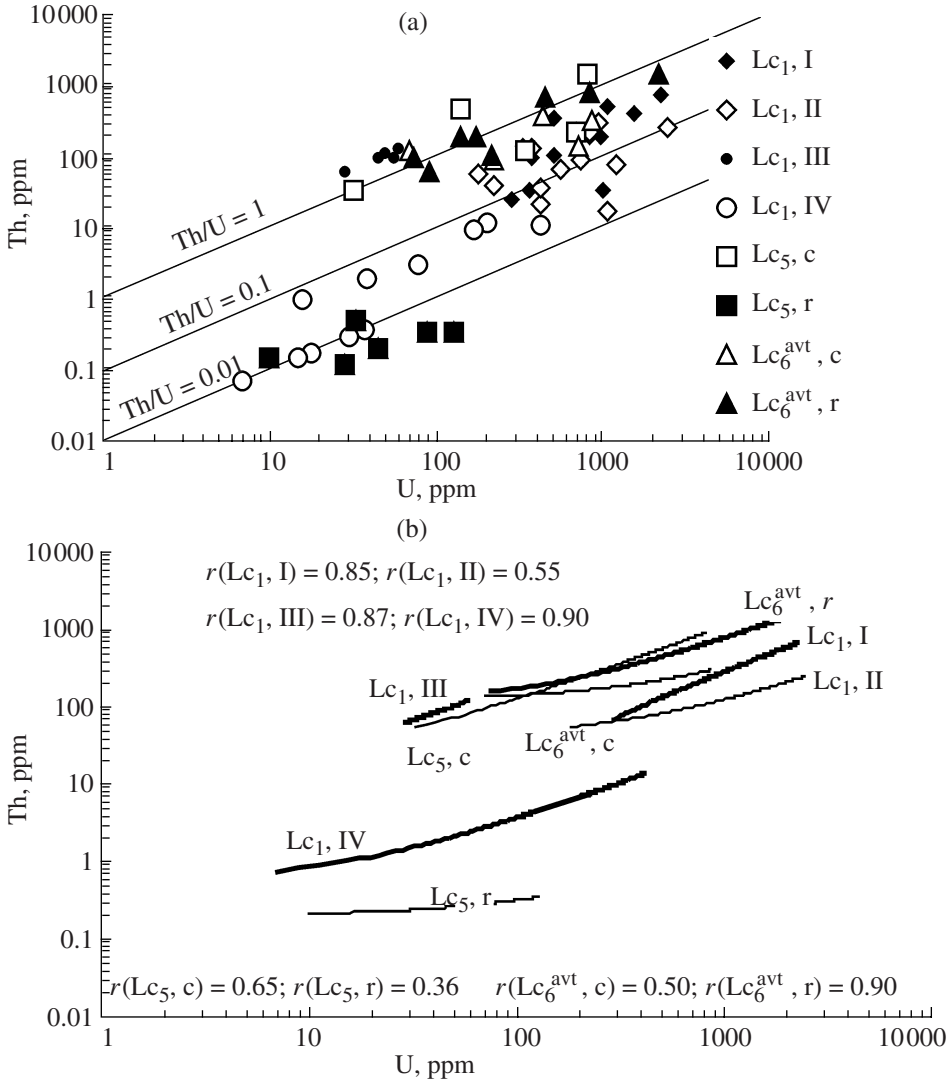

Fig. 4. Th–U diagram for zircons from samples of Lc_1 (sample 1515d/1), Lc_5 (1264a), Lc_6^{avt} (1274o). I, II, III, and IV are phases (types) of zircon in Lc_1, c and r are the cores and rims of zircon grains, respectively, from granites Lc_5 and Lc_6^{avt}. The diagram in Fig. 4b shows the trends of the zircons and the correlation coefficients *r*, which are printed in a semibold face at a significance level of 0.05.

10 spots. It can be readily noted that the isotopic-composition points of zircon from granite-gneiss Lc_1 (sample 1515d/1) define three clusters in the diagram of Fig. 6, with these clusters corresponding to at least three distinct major geological events separated by significant time spans.

As could be expected, the rhythmically zonal cores (type I) mostly yield discordant isotopic ratios that cannot be accurately enough approximated by a linear dependence. The core of one zircon of type I with the minimum discordance of 1% gave an age of 2964 ± 13 Ma (Fig. 6). Spots 1.6.2, 1.12.1, and 4.1, which correspond to various degrees of alteration of zircon with the oldest $^{207}Pb/^{206}Pb$ age were used to construct a discordia, whose upper intercept with the concordia corresponds to an age of 3010 ± 20 Ma. This value can be interpreted as the age of the protolith. It should be mentioned that the accuracy of these determinations is relatively low. Nevertheless, this age estimate is reliable in the sense that it significantly differs from the age values of zircons of other types.

Another group of points near the concordia (Fig. 6) represents zircons of types II and III. The concordant age calculated for four nearly concordant points for type-II zircons is equal to 2677 ± 16 Ma. Zircons of type III yielded a concordant age of 2703 ± 20 Ma, which can be interpreted as the age of metamorphism and granitization (development of the Stanovoi granite-

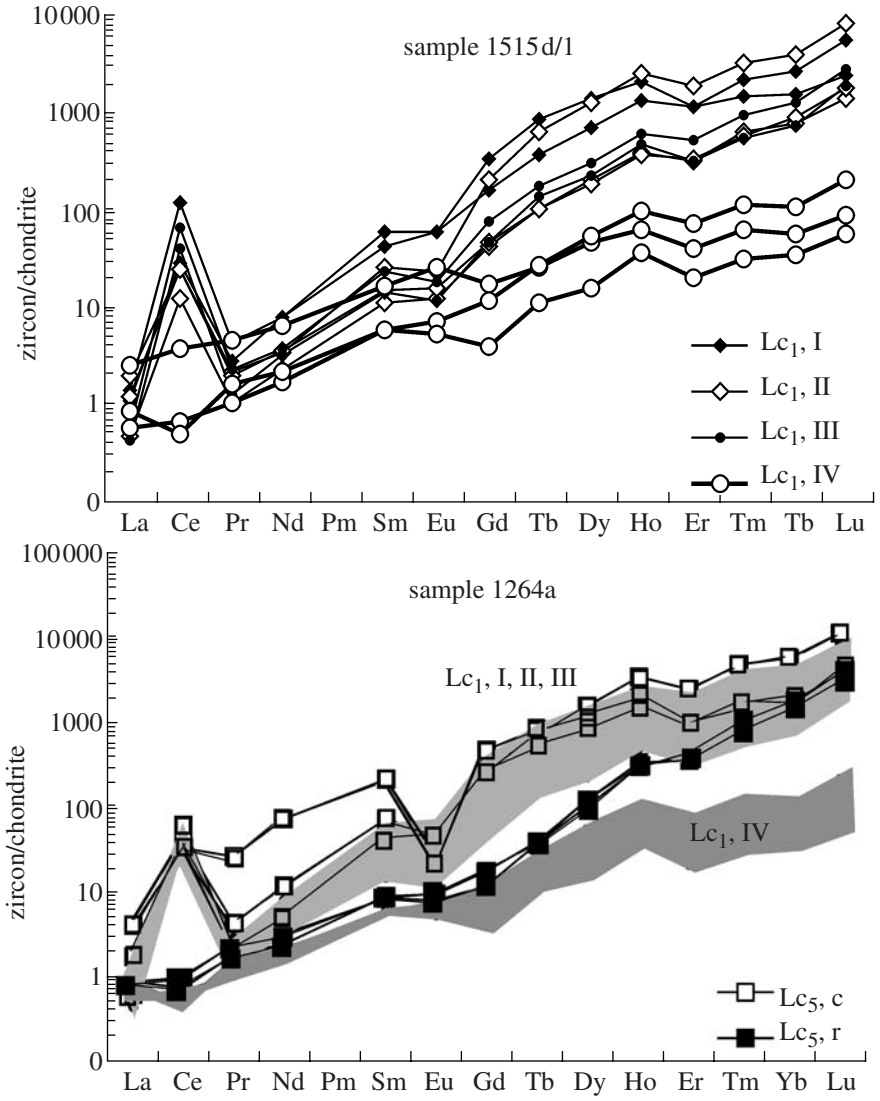

Fig. 5. Chondrite-normalized (Boyton, 1984) REE patterns of zircons from (a) Lc_1 (sample 1515d/1) and (b) Lc_5 (sample 1264a). See note to Fig. 4 for the designations of zircon types.

gneisses). Note that analogous age values were obtained on zircons that notably differ from others in geochemistry. The REE, U, and Th concentrations in zircons of type II are close to those in zircons of type I. The reason for this is the fact that type-II zircons crystallized via the replacement of old cores and inherited their geochemical features, while the isotopic ratios of these zircons correspond to the new geological event. In contrast to zircons of this type, zircons of type III occur as individual crystals.

The third group of points, which plot near the concordia, corresponds to zircons of type IV. The concordant age values calculated on six zircon compositions with low discordance (±1%) is 1915 ± 7 Ma (Table 2, Fig. 6). The data points are widely spread along the concordia, so that the error can be significantly underestimated. This age value may correspond to the development of the imbricated nappe structure. This event strongly affected the area in question, as follows from the fact that this zircon type is predominant in sample 1515d/1. Another remarkable feature of zircon from this sample is the absence of rims having an age younger than 1915 ± 7 Ma.

It is now pertinent to discuss the dates yielded by vein granites Lc_5, which were provisionally correlated (based on geological evidence) with the Late Stanovoi granites (Table 3, Fig. 7) and developed after the imbricated nappe structure was formed, in relation to deformations overprinting it. The long-prismatic zircons yielded relatively stable $^{206}Pb/^{238}U$ age values within the range of 136–149 Ma. These variations lie within the errors of the individual measurements. The situation is more complicated with the cores. Three values of their $^{206}Pb/^{238}U$ ratio fall within the range of 216–222 Ma,

Table 3. Isotopic data on zircons from vein granite Lc_5 (sample 1264a)

Spot	Zircon type	Concentration					Age, Ma	Isotopic ratios								Err corr
		$^{206}Pb_c$, %	U, ppm	Th, ppm	$^{232}Th/^{238}U$	$^{206}Pb^*$, ppm	$^{206}Pb/^{238}U$	$^{238}U/^{206}Pb^{*1}$	±, %	$^{207}Pb^*/^{206}Pb^{*1}$	±, %	$^{207}Pb^*/^{235}U^1$	±, %	$^{206}Pb^*/^{238}U^1$	±, %	
3.1*	r	3.62	91	0.33	0.004	1.64	129 ± 4	49.50	3.3	0.042	52	0.118	53	0.0202	3.3	0.064
7.2	r	8.52	10	0.15	0.02	0.20	136 ± 11	47.00	7.8	0.069	79	0.200	79	0.0213	7.8	0.099
3.1	r	2.33	130	0.34	0.003	2.48	138 ± 3	46.20	2.5	0.044	30	0.133	30	0.0216	2.5	0.084
5.1	r	3.19	34	0.52	0.02	0.67	142 ± 6	44.90	4.4	0.047	64	0.144	64	0.0223	4.4	0.068
4.1	r	4.22	45	0.20	0.005	0.91	143 ± 4	44.50	2.7	0.047	32	0.146	32	0.0225	2.7	0.083
6.2	r	5.64	29	0.12	0.004	0.61	149 ± 6	42.80	4.4	0.045	67	0.144	67	0.0234	4.4	0.065
3.2	c	3.27	33	35	1.12	0.99	216 ± 6	29.33	3.0	0.051	37	0.238	37	0.0341	3.0	0.083
6.1	c	0.90	825	1489	1.87	24.90	221 ± 2	28.69	0.7	0.050	3.9	0.240	3.9	0.0349	0.7	0.184
7.1	c	0.23	343	127	0.38	10.30	222 ± 2	28.58	0.8	0.050	3.1	0.242	3.2	0.0350	0.8	0.248
1.1	c	0.01	143	493	3.57	42.00	1900 ± 14	2.92	0.8	0.113	0.9	5.330	1.2	0.3428	0.8	0.670
2.1	c	0.01	707	227	0.33	271.00	2376 ± 12	2.24	0.6	0.177	0.4	10.892	0.7	0.4456	0.6	0.865

Note: See note to Table 2. The calibration error is 0.28%; c and r denote the cores and rims of mineral grains, respectively.

Table 4. Isotopic data on zircons from leucosome Lc_6 (sample 12740)

Spot	Zircon type	Concentration					Age, Ma	Isotopic ratios								Err corr
		$^{206}Pb_c$, %	U, ppm	Th, ppm	$^{232}Th/^{238}U$	$^{206}Pb^*$, ppm	$^{206}Pb/^{238}U$	$^{238}U/^{206}Pb^*$	±, %	$^{207}Pb^*/^{206}Pb^*$	±, %	$^{207}Pb^*/^{235}U$	±, %	$^{206}Pb^*/^{238}U$	±, %	
5.2	r	0.24	2233	1553	0.72	35.4	117.5 ± 0.6	54.24	0.5	0.0500	1.4	0.12	3.0	0.0184	0.5	0.172
3.1	r	3.70	74	100	1.39	1.2	117.9 ± 4.2	52.19	2.3	0.0707	6.8	0.10	57.0	0.0185	3.6	0.064
2.1	r	0.75	143	201	1.45	2.3	120.9 ± 2.0	52.42	1.6	0.0573	5.4	0.13	10.2	0.0189	1.7	0.167
4.1	r	0.43	845	859	1.05	13.9	122.1 ± 1.0	52.07	0.8	0.0498	2.3	0.12	4.0	0.0191	0.8	0.198
2.2	r	2.54	92	64	0.72	1.6	123.8 ± 4.1	50.25	2.0	0.0666	9.4	0.12	48.6	0.0194	3.4	0.069
1.2	r	1.84	217	109	0.52	3.7	124.1 ± 2.4	50.51	1.3	0.0527	6.4	0.10	31.7	0.0194	1.9	0.061
5.1	r	0.38	460	710	1.60	7.7	124.3 ± 1.3	51.19	1.0	0.0503	3.0	0.13	5.7	0.0195	1.1	0.188
1.1	r	0.78	174	201	1.19	3.0	128.4 ± 1.9	49.32	1.4	0.0528	4.9	0.13	10.1	0.0201	1.5	0.152
7.2	c	0.12	71	127	1.83	1.2	1254.4 ± 13.3	4.65	1.2	0.1108	1.7	3.25	2.1	0.2148	1.2	0.542
8.1	c	0.12	226	94	0.43	73.3	2059.2 ± 11.1	2.65	0.6	0.1564	0.6	8.06	1.0	0.3763	0.6	0.637
6.1	c	–0.02	723	141	0.20	265.6	2295.1 ± 7.9	2.34	0.4	0.1840	0.3	10.86	0.5	0.4276	0.4	0.800
7.1	c	–0.02	441	401	0.94	182.1	2530.9 ± 36.8	2.08	1.8	0.1829	0.4	12.14	1.8	0.4808	1.8	0.978
9.1	c	0.02	867	347	0.41	361.8	2552.4 ± 7.0	2.06	03	0.1925	0.3	12.88	0.4	0.4858	0.3	0.779

Note: See notes to Tables 2 and 3.

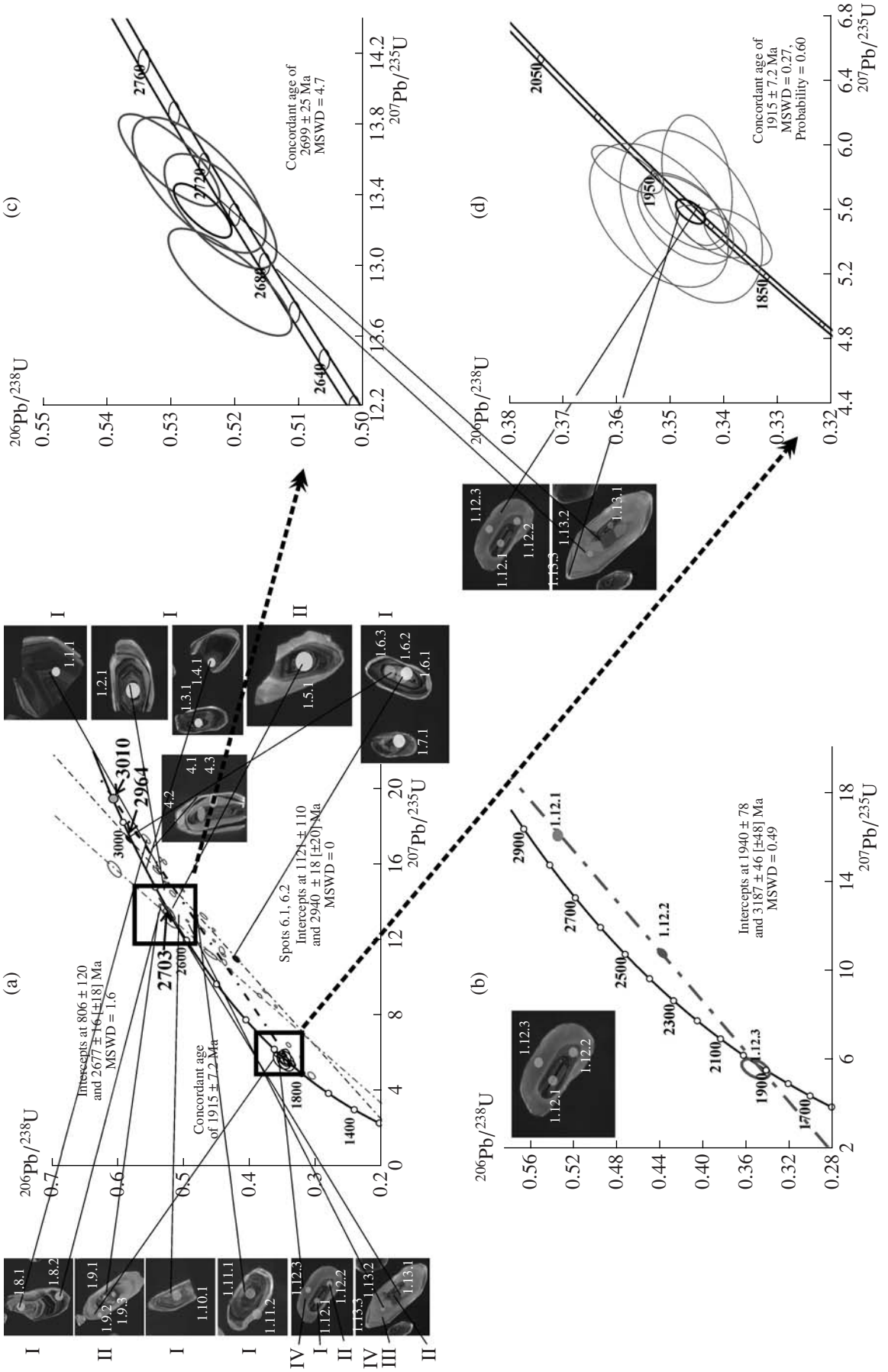

Fig. 6. Concordia diagrams for zircons from Stanovoi plagiogneisses Lc_1 (sample 1515d/1).
The diagrams show (c, d) the calculated concordant age and (a, b) age determined by concordia and discordia intercepts. Ovals printed in a semibold face are concordant age values for single grains.

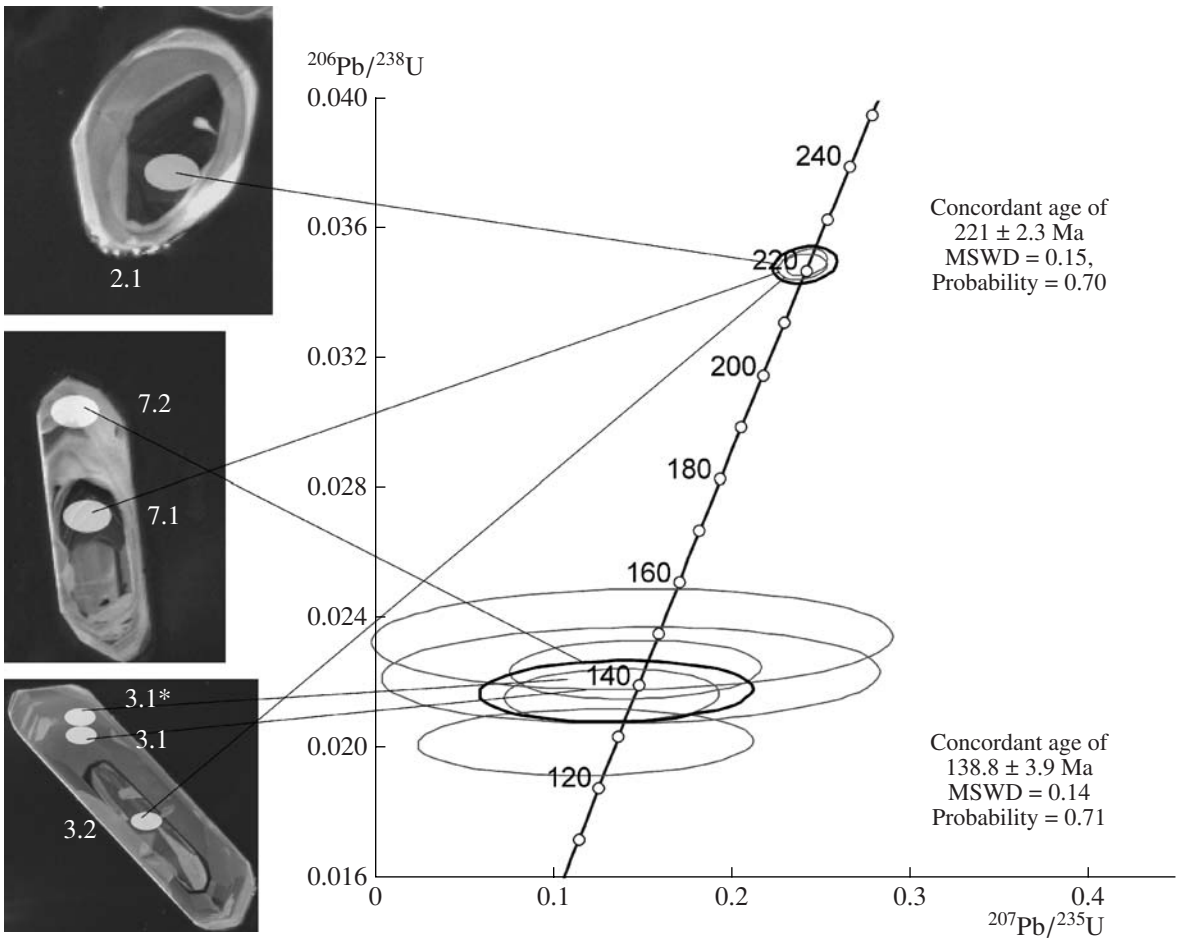

Fig. 7. Concordant age of zircons from granites Lc_5 (sample 1264a).
Ovals printed in a semibold face are concordant age values for single grains.

and two cores have an Early Precambrian age, with the date of 1900 Ma characterized by high concordance, and the date of 2300 Ma significantly deviating from the concordia and having no geological sense. Conceivably, the age of the long-prismatic grains corresponds to the crystallization age of the granite from melt.

Data on sample 1274o (Table 4, Fig. 8) definitely indicate that the melt of leucosome Lc_6^{avt} crystallized between 127 and 130 Ma, which is consistent with geological observations.

GEOCHEMISTRY OF MAJOR AND TRACE ELEMENTS

Major elements. We have previously studied the petrochemistry of the protolithic rocks and leucosomes of migmatites of population 7 based on 152 chemical analyses (Glebovitsky and Sedova, 1984; Sedova and Glebovitsky, 1985, 1987). The average compositions presented herein were calculated taking into account 27 newly obtained analyses (Table 5). The group of mafic rocks includes original crystalline schists (*Sch*), and the group of migmatized schists (*Sch**) includes variably migmatized rocks. The protolithic basic rocks are amphibole–plagioclase crystalline schists and amphibolites (rarely, with diopside), whose SiO_2 contents vary from 45 to 59 wt % (in 26 samples of 27). Not dwelling on the characteristics of their composition, we would only like to mention that, according to their Al_2O_3–(FeO* + TiO_2)–MgO proportions, the rocks belong to the calc–alkaline series. According to the classification based on proportions of the sum of alkalis and silica (*Classification…*, 1981), this group is dominated by basalts and trachybasalts (13 samples of 27), with less abundant basaltic andesites and trachybasaltic andesites (9 samples), andesites (4 samples), and dacites (1 sample); 63% of the analyzed samples for which a simultaneous increase in the K_2O and Na_2O concentrations is typical belong to the subalkaline series ($Na_2O + K_2O > 4.5$–8 wt %). In the K_2O–SiO_2 diagram, ten samples plot within the field of the shoshonite series. Six samples fall into the field of high-K series in the field of moderate-K series (Efremova and Stafeev, 1985). The Fe mole fraction (Fe#) of these rocks varies from 40 to 60%, their degree of Fe oxidation (f_0) ranges

from 20 to 30%, and the ASI ranges from 0.4 to 0.9 (with most samples lying within the range of 0.8–0.9). The correlations revealed between elements are typical of rocks of intermediate–basic composition: Si is negatively correlated with Ti + Mg + Fe* and Ca (Fig. 9a), as well as with Fe^{3+}, Fe^{2+}, Mn, and Mg and is positively correlated with Na at the absence of significant correlations with K, Ti, and Al (Fig. 9a).

The group of biotite (sometimes with hornblende) plagiogneisses and granite-gneisses (Lc_1) comprises varieties of composition ranging from tonalite and trondhjemite to granodiorite and granite, with the predominance of varieties containing 68–73 wt % SiO_2 (Table 6). In terms of *Ab–An–Or* proportions, the most widely spread rocks are trondhjemites, whereas tonalites and granites occur in roughly equal amounts (Table 6). An increase in the sum of alkalis is accompanied by an increase in the content of K_2O and a decrease in the concentration of Na_2O (correlation coefficient r for K_2O and Na_2O is –0.60). Most samples have ASI within the range of 0.9–1.2, with most samples lying within the ASI range of 1–1.1; Fe# varies mostly from 50 to 70% (with most samples occurring within the range of 20–30%). Si is negatively correlated with Ti + Mg + Fe*, Al and Ca (Fig. 9a).

Leucosomes Lc_2 always contain >68 wt % SiO_2, are dominated by trondhjemites, but the percentage of granites increases and that of tonalites decreases relative to those in Lc_1 (Table 6). The correlation between K and Na is negative (r = –0.58). The most widely spread rocks have ASI of 1.0–1.1 and 1.2–1.3. According to variations in Fe# and f_0, the rocks are close to Lc_1 but are less mafic and include more varieties with higher sums of alkalis. Si is negatively correlated with Al, Ti + Fe* + Mg (Fig. 9b), and also with Fe^{2+} and Mg. The composition of leucosomes Lc_3 is analogous to that of Lc_1 and is more mafic and less silicic than that of Lc_2. Many parameters of Lc_4 are analogous to those of Lc_2, although Lc_4 includes more granites. Lc_4 does not exhibit any significant correlation between K and Na, as in the previous rock group, and between Si and major elements, except Al (Fig. 9b). A remarkable features of the rocks is their even distribution within three ASI intervals (1.0–1.1, >1.1–1.2, and >1.2–1.3) and a pronounced maximum in the number of samples within the ranges Fe# = 60–70% and f_0 = 20–30%.

Granites Lc_5 are the most leucocratic of all of the groups. Their SiO_2 contents range from 69.5 to 73.83 wt %, and the fraction of grains in this group amounts to 71% (Table 6). The ASI values of the rocks are always greater than 1.0. The maximum of our samples fall within the Fe# range of 60–70%, and their f_0 varies from 2 to 58%. The rocks are characterized by the absence of correlations between Si and other elements (except Al and Ti + Mg + Fe*) (Fig. 9c). Na and K show a negative correlation (r = –0.75).

The group Lc_6^{avt}, whose protolithic rocks were migmatites, plagiogneisses, and crystalline schists, is characterized by geometries of the bodies and compositional features most closely resembling those of Lc_1 (Table 5) but differs from the latter in including a higher percentage of tonalites and more varieties with SiO_2 < 68 wt % (Table 6), which is likely explained by the impossibility of recognizing an intermediate rock group because of the ubiquitous and close alternation of varieties. Compared to group Lc_1, Lc_6^{avt} more often includes amphibole-bearing rocks, which is the likely reason for the equally frequent occurrence of varieties with ASI = 0.9–1.0 and 1.0–1.1. The Fe# varies from 50 to 80%, f_0 = 20–30%; Si is negatively correlated with Ti + Mg + Fe*, Al, and Ca (Fig. 9c); and Na and K are also negatively correlated with each other (r = –0.74). Lc_6^{all}, which were produced by the further transformation of Lc_6^{avt} are richer in Si and K, are less mafic (Tables 5, 6), and include more granites. The Fe# of Lc_6^{all} mostly ranges from 50 to 70%, f_0 = 10–30%, ASI = 0.9–1.1. Negative correlations were identified between Si and Ti + Mg + Fe* and between K and Na (r = –0.53). It cannot be ruled out that the most silicic varieties belong to Lc_7.

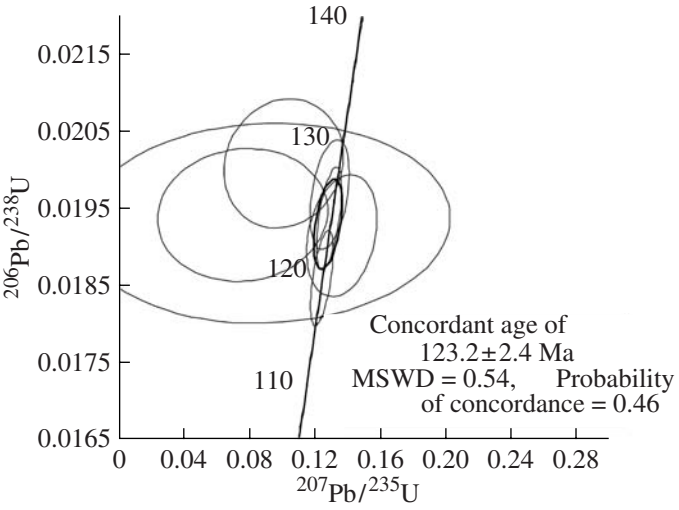

Fig. 8. Concordia diagram for zircons from tonalite gneiss Lc_6^{avt} (sample 1274o).

The character of transformation of the basic rocks during their granitization and the development of leucosomes is clearly illustrated in variation diagrams (Fig. 9) and can be seen when the average major-element compositions of the rock groups are compared. The origin of Lc_1 is associated with a systematic increase in the contents of Si, Na, and K at a decrease in the concentrations of mafic elements and P (Table 5). This trend is also characteristic of Lc_2 and Lc_4 (in which only the Na and K concentration do not change) but is disturbed in Lc_3 (higher basicity and an increase

Table 5. Average composition (wt %) of rocks from the lower and middle reaches of the Nyukzha River

Oxide	*Sch*	*Sch**	*Mig*	Lc_1	Lc_2	Lc_3	Lc_4	Lc_5	Lc_6^{avt}	Lc_6^{all}
	52.83 4.61	62.26 4.25	64.51 4.14	69.88 3.20	72.83 1.95	69.41 1.76	72.23 2.85	71.88 1.59	67.50 4.13	70.33 1.89
TiO_2 x	1.09	0.65	0.60	0.39	0.18	0.25	0.19	0.28	0.40	0.33
σ	0.58	0.22	0.20	0.24	0.10	0.11	0.13	0.21	0.17	0.13
Al_2O_3 x	15.92	15.68	15.76	15.23	14.99	15.86	15.02	15.48	15.94	15.10
σ	1.90	1.19	0.69	0.85	0.95	0.60	1.79	1.10	0.84	0.82
Fe_2O_3 x	4.62	2.82	2.61	1.64	0.96	1.18	1.09	0.57	1.70	1.04
σ	2.68	1.20	1.59	1.22	0.67	0.69	1.00	0.50	0.81	0.73
FeO x	5.72	3.75	3.02	1.79	1.08	1.51	1.22	0.91	1.95	1.49
σ	1.32	1.05	0.98	0.68	0.39	0.66	0.70	0.36	0.76	0.62
MnO x	0.14	0.12	0.09	0.05	0.03	0.05	0.03	0.03	0.06	0.04
σ	0.05	0.06	0.02	0.02	0.02	0.02	0.02	0.01	0.03	0.02
MgO x	4.91	2.66	1.99	1.01	0.48	0.90	0.43	0.37	1.47	0.75
σ	2.32	1.21	0.87	0.43	0.27	0.69	0.24	0.12	0.94	0.32
CaO x	7.49	4.97	4.18	2.71	1.84	2.63	1.97	1.28	3.52	2.26
σ	2.64	1.40	1.08	1.06	0.41	1.17	0.68	0.59	1.32	0.95
Na_2O x	3.44	3.88	4.28	4.16	4.13	3.70	4.14	4.54	3.97	3.63
σ	1.04	0.57	0.51	0.51	0.63	0.80	0.85	0.86	0.42	0.36
K_2O x	1.96	1.91	2.13	2.43	2.56	3.60	2.90	3.71	2.60	3.87
σ	0.85	0.77	0.61	1.32	1.59	2.44	1.53	1.05	1.26	1.32
P_2O_5 x	0.34	0.25	0.20	0.11	0.05	0.06	0.05	0.06	0.11	0.08
σ	0.29	0.23	0.13	0.10	0.03	0.02	0.04	0.03	0.08	0.03
LOI x	1.82	1.17	1.00	0.82	0.56	0.55	0.58	0.51	0.80	0.74
σ	0.83	0.53	0.32	0.46	0.26	0.18	0.36	0.19	0.37	0.30
Total x	99.87	100.11	100.04	99.97	99.44	99.59	99.56	99.59	100.02	99.67
σ	0.72	0.39	0.40	0.67	0.65	0.76	0.58	0.54	0.70	0.67
N	27	21	9	26	20	8	14	14	23	17

Note: *N* is the number of analyses, x is the average; σ is the standard deviation; *Sch* and *Sch** are basites and granitized basites, respectively, *Mig* are migmatites, Lc_1 are plagiogneisses and granite-gneisses, Lc_2, Lc_3, and Lc_4 are the leucosomes of the second, third, and fourth populations, Lc_5 is granites composing small stromatic and cutting bodies in the field of Lc_1; Lc_6^{avt} is tonalite gneisses, Lc_6^{all} is granitoids in the field of Lc_6^{avt}.

in the K concentration). The average Si, Al, Fe^{2+}, and Mg concentrations in the latter are close to those in Lc_1, which is explained by the derivation of Lc_3 via the mobilization of Lc_1. The development of Lc_6^{avt} after basic rocks, migmatites, and Lc_1 and the subsequent origin of Lc_6^{all} and Lc_6^{avt} are accompanied with changes in composition analogous to those during the development of Lc_1 and Lc_2. Granites Lc_5, which often plot within the field of Lc_1, are poorer in Mg and Ca and richer in alkalis than the other leucosomes.

Trace elements. The trace-element (including REE) geochemistry of the rocks was studied based on 53 samples, which were analyzed by ICP-MS. Table 7 illustrates significant variations in the concentrations of these elements in rock groups and trends of these concentrations in the process of ultrametamorphism. Some samples in group Lc_1 have very high concentrations of LREE (three samples of the eleven), HREE (two samples), and Eu, Zr, Hf, Ta, Nb, Y, and Zn. This is usually caused by the enrichment of the rocks in accessory minerals, including allanite, sphene, zircon, and apatite. This follows from temperature estimates on Zr (Watson and Harrison, 1983), which strongly vary and are obviously overestimated for Lc_1 and Lc_2, reaching 840–890°C at Zr concentrations of 260–570 ppm, i.e., extend outside the amphibolite facies. The most probable reason for this is the entrapment of zircon from protolithic rocks. Below we discuss an increase or decrease in the concentrations of elements or their ratios in a rock sequence only if these changes are statistically significant, which can be tested by the Van der Varden criterion at an assumed significance level of 0.05. System-

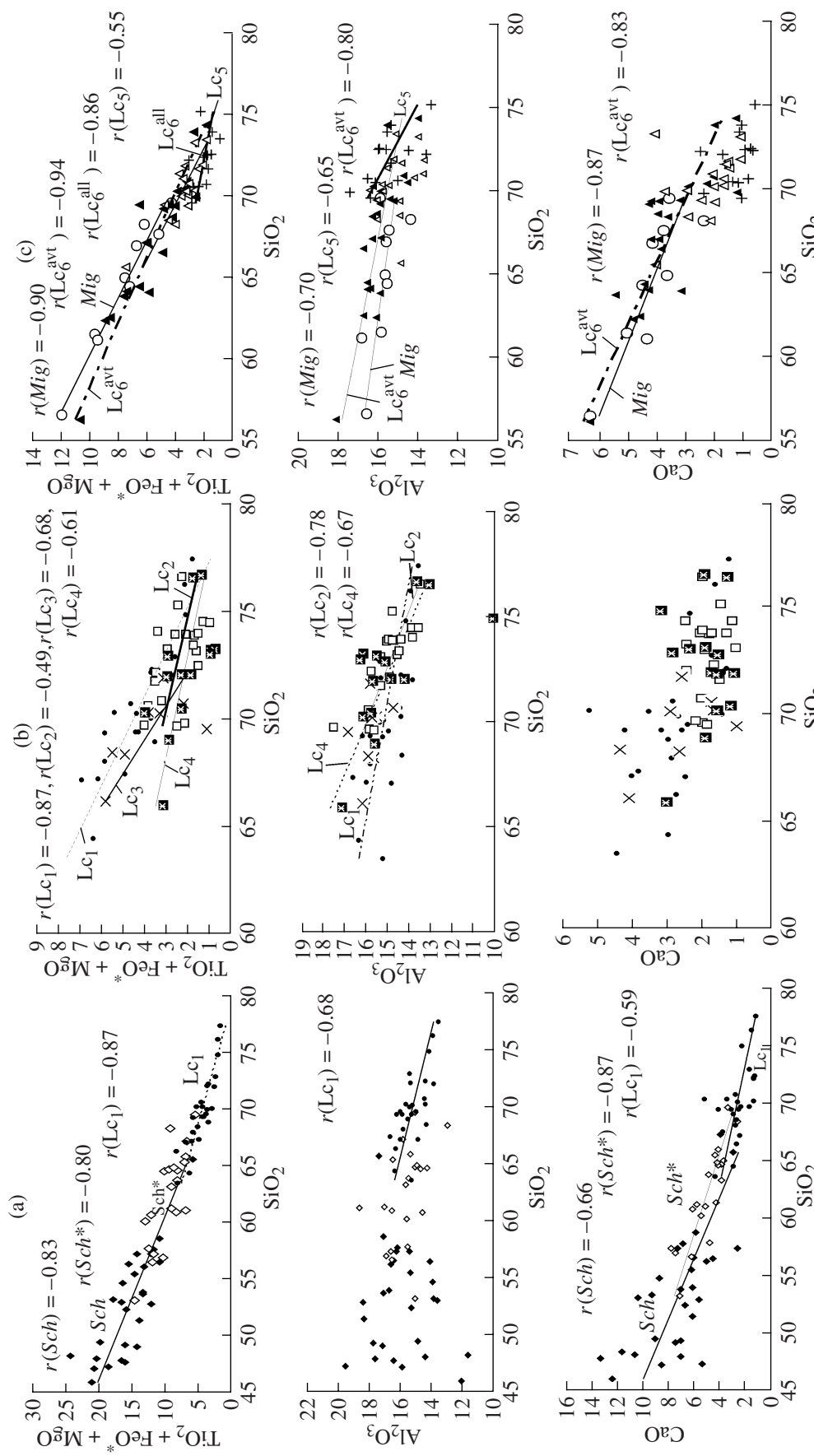

Fig. 9. Variation diagrams for (a) crystalline schists *Sch*, granitized schists *Sch**, and granite-gneisses Lc_1; (b) granite-gneiss Lc_1, leucosomes of migmatites Lc_2, Lc_3, Lc_4; and (c) migmatites *Mig*, granites Lc_5, tonalite gneisses Lc_6^{avt}, and the leucosomes of network migmatites Lc_6^{all}. The diagrams show statistically significant (at a significance level of 0.05) values of correlation coefficients *r* and the trends.

Table 6. Distribution (%) of analyzed granitoid samples according to their SiO_2 concentrations and the *Ab–An–Or* proportions

Characteristics	Lc_1 (26)	Lc_2 (20)	Lc_3 (8)	Lc_4 (14)	Lc_5 (14)	Lc_6^{avt} (23)	Lc_6^{all} (17)
< 68 wt % SiO_2	23		12	7		43	6
68–73 wt % SiO_2	65	40	88	57	79	48	82
> 73 wt % SiO_2	12	60		36	21	9	12
Tonalite, %	19	15	25	7	22	48	12
Trondhjemite, %	39	50	25	29	7	4	
Granodiorite, %	19					22	23
Quartz monzonite, %						9	
Granite, %	23	35	50	64	71	17	65

Note: Numerals in parentheses correspond to the number of samples.

atic variations can be identified at a lower significance level.

The basic rocks have REE patterns typical of mafic volcanics: weakly differentiated and without Eu anomalies (Fig. 10a). The fractionation of REE becomes stronger in gneisses Lc_1 (Fig. 10a), the La/Yb ratio and LREE contents increase, whereas the concentrations of HREE decrease; six of the eleven samples have Eu/Eu* > 1. The leucosomes of the anatectic migmatites (Lc_2, Lc_3, and Lc_4) contain less LREE and HREE and have lower La/Yb and higher Eu/Eu* and Sm/Nd ratios (Figs. 10b, 10c). Simultaneously with the increase in the REE concentrations from the basic rocks to granite-gneisses Lc_1, the latter rocks become enriched in Th, Zr, and Hf, while the younger leucosomes are depleted in these elements. Populations of leucosomes Lc_2 and Lc_4 have similar concentrations of these elements, and Lc_3 differs from them in having low concentrations of these elements. Another trend in the average concentrations is typical of LILE: the concentrations of Rb, Ba, Sr, and Pb systematically increase in the succession *Sch* ⟶ Lc_1 ⟶ Lc_2 ⟶ Lc_3 ⟶ Lc_4, while the concentrations of HFSE (Nb, Ta, and Y) and transition elements (Co, Cr, Ni, and V) decrease. The trends of the REE, Li, Be, and Ba concentrations are violated in Lc_3. Granite veins Lc_5 are represented only by three samples and are heterogeneous: their $(La/Yb)_n$ ratio varies from 53 to 103, Eu/Eu* = 1–1.3, LREE = 48–85, and HREE = 1.0–3.3 (Fig. 10d). These rocks differ from all other leucosomes in bearing high Sr concentrations (Table 7). It is interesting that these granites are the most leucocratic, most silicic, and most potassic, which makes them principally different from Lc_6^{avt}. The average Nb, Zr, Hf, LREE, and Eu concentrations of granites Lc_5 are close to those in Lc_6^{avt}, but the former have higher Rb, Ba, Sr, and Ta concentrations and are remarkably poorer in Co, V, Ni, Cr, and HREE.

The products of the late (Cretaceous) granitization developed after mafic rocks, migmatites, and Lc_1 after the origin of all leucosome populations and are, in turn, replaced by Lc_6^{all}. Lc_6^{avt} are characterized by lower REE concentrations relative to those in the protolithic rocks (Fig. 10e). Some elemental ratios vary in the rock succession protolith ⟶ Lc_6^{avt} ⟶ Lc_6^{all} as follows: $(La/Yb)_n$ – 10.5–42.6 ⟶ 12.1–61.7 ⟶ 24.3–37.3, Eu/Eu* – 0.9–1.4 ⟶ 1.1–1.4 ⟶ 0.7–1.6; Sm/Nd – 0.13–0.21 ⟶ 0.13–0.23 ⟶ 0.13–0.16. The REE patterns of Lc_6^{avt} and Lc_6^{all} are different: the latter rocks are richer in REE at La/Yb ratios close to those in the former (Fig. 10f). Lc_6^{all} are significantly richer in Nb and Ta than all other granitoids.

Basic understanding of the general evolution of the granite-forming processes can be gained through comparing Lc_1 with Lc_6^{avt}, all of which were formed early in the course of the processes in question and which share many specific morphological features. In our series of samples, Lc_1 replace crystalline schists *Sch* of mafic–intermediate composition (eleven series), and Lc_6^{avt} develop after migmatites (two series), granite-gneisses Lc_1 (three series), and crystalline schists *Sch* (one series). In spite of the significant differences in the composition of the protolithic rocks, Lc_1 show statistically significant differences from Lc_6^{avt} only in high LREE and Rb concentrations (Fig. 11) and high La/Yb ratios. This seems to be a tendency toward higher concentrations of Nb, Ta, Zr, Hf, Th, Y, Sr, Ba, and LREE in Lc_1 than Lc_6^{avt} (Table 7). It is also worth noting that analogous tendencies in the behavior of relatively little mobile elements (except Ba and Th) were identified in the protolithic rocks of Lc_1 and Lc_6^{avt}, a fact that can be considered testifying that the migmatization products inherit their composition from the protoliths.

Younger allochthonous granites Lc_6^{all} can have a genesis similar to that of leucosome populations, most probably Lc_3. Granites Lc_6^{all} have concentrations of major elements similar to those in Lc_3 (Table 5) but notably differ from the latter rocks and from Lc_2 and Lc_4 in containing higher concentrations of LREE, HREE, Eu, Y, Zr, Hf, Th, Ta, Nb, U, V, Co, Ni, and Zn at lower concentrations of Ba and Sr and similar concentrations of Rb and Pb (Table 7).

The concentrations of elements in the leucosomes normalized to those in their protoliths can be used as a measure of the intensity of transformations in the pro-

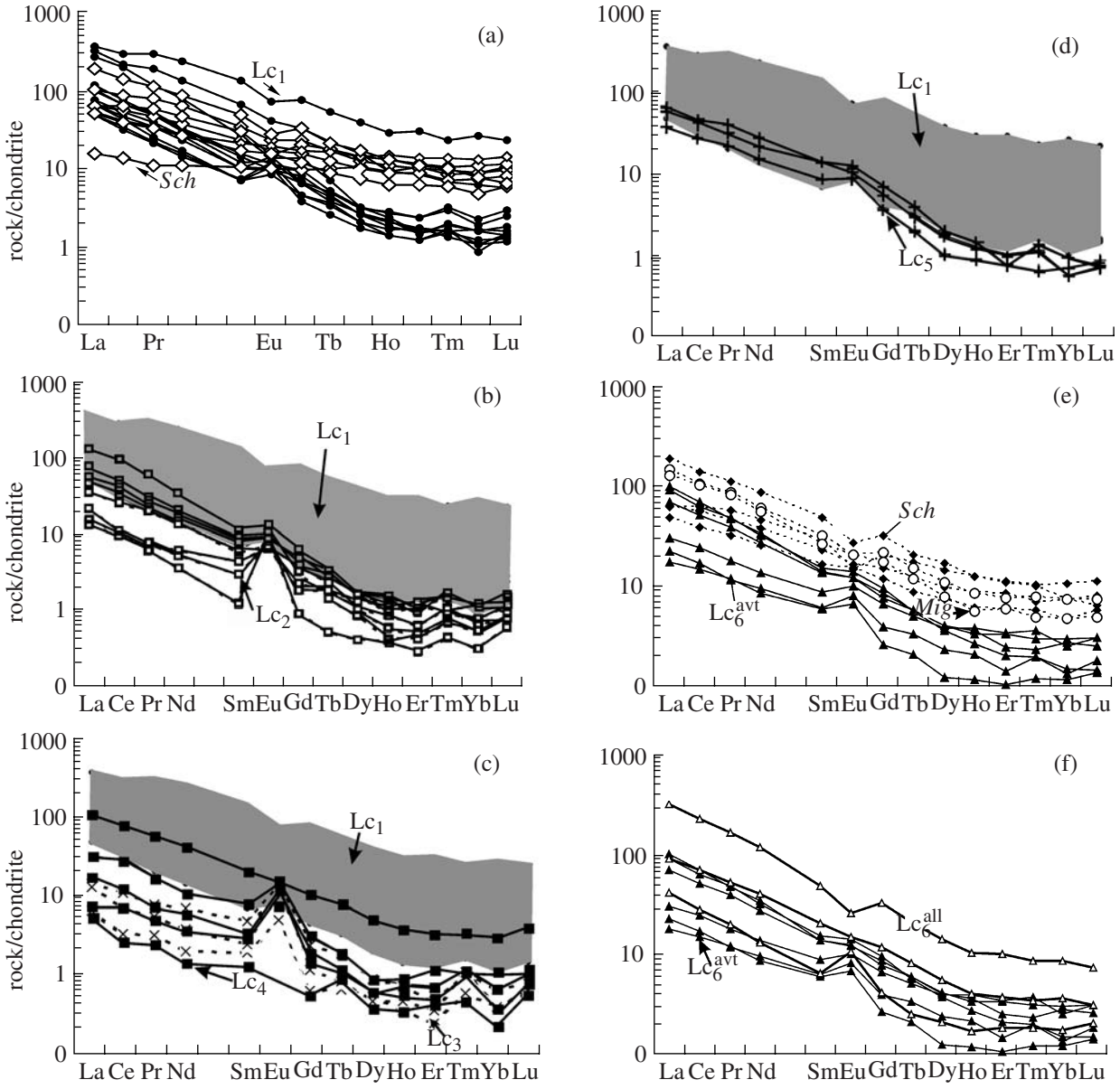

Fig. 10. Chondrite-normalized (Boyton, 1984) REE patterns of the rocks. Rock group abbreviations are shown in Fig. 9. Gray field denotes Lc_1.

tolithic rocks during each stage of ultrametamorphism. Table 8 lists average values of these ratios for discrete stages of these processes and the number of series in which an increase or decrease in the concentrations of elements was detected in the ultrametamorphic products. When Lc_1 and Lc_6^{avt} develop after different protoliths, some elements show systematic statistically significant variations in their concentrations with different degrees of enrichment or depletion. For example, when Lc_1 develops, Ba is more significantly introduced than during the origin of Lc_6^{avt}, while V, Cr, Co, Ni, Li, HREE, and Y are more significantly removed. The changes in the concentrations of Rb, LREE, Eu, Zr, Hf, and Th have different signs in Lc_1 and Lc_6^{avt}: these elements are enriched in the former and depleted in the latter.

Significant differences in the character of changes in concentrations were determined during the comparison of granitization and partial melting successions *Sch* ⟶ Lc_1 and protolith ⟶ Lc_2, Lc_3, Lc_4, respectively. For example, LREE, Zr, Hf, and Th show changes in their concentrations of different sign: their concentrations increase in the former series and decrease in the latter. V, Cr, Co, Ni, and Sc are characterized by the same signs of changes: their concentrations decrease in both series, although more significantly during the development of Lc_1. Other elements

Table 7. Average concentrations (ppm) of trace elements in crystalline schists (basites) and ultrametamorphic products developing after them in the lower and middle reaches of the Nyukzha River

Element	*Sch* (7)	*Mig* (3)	Lc_1 (11)	Lc_2 (9)	Lc_3 (4)	Lc_4 (5)	Lc_5 (3)	Lc_6^{avt} (6)	Lc_6^{all} (3)
Li x	13.68	20.65	12.04	4.44	2.38	4.05	11.77	8.68	8.18
σ	8.41	12.26	6.94	2.46	1.72	2.28	10.88	4.18	3.38
Be x	1.31	1.58	1.15	1.10	1.44	1.04	2.2	1.2	1.75
σ	0.38	0.71	0.49	0.41	0.95	0.40	0.77	0.18	0.29
Cs x	1.06	1.28	1.14	0.62	0.54	0.94	0.56	0.72	1.00
σ	0.75	0.81	1.08	0.55	0.70	0.57	0.24	0.42	0.09
Rb x	50.0	59.8	57.0	51.4	73.8	76.6	50.4	39.6	88.1
σ	27.3	21.9	19.4	26.2	30.1	25.2	36.6	23.4	28.1
Ba x	551	631	1236	1699	6477	5463	1699	1043	1861
σ	300	79	668	522	8531	7653	670	484	262
Sr x	779	622	1223	1474	1534	1680	4812	1006	902
σ	245	237	713	1013	1439	988	1421	374	25
Pb x	7.12	7.47	9.35	9.82	12.25	12.17	11.08	7.87	13.53
σ	1.27	0.53	2.93	3.19	3.00	5.14	2.74	1.35	4.93
Ga x	18.7	19.9	16.5	13.8	13.8	13.4	18.1	16.2	16.5
σ	2.4	2.4	1.9	1.1	1.3	2.4	3.7	1.2	1.8
Sc x	25.5	9.3	3.6	0.7	0.8	1.3	0.9	5.0	4.9
σ	8.7	6.4	2.6	0.5	1.2	2.0	0.3	2.6	7.0
V x	194	109	51	20	17	18	24	45	40
σ	64	58	13	8	14	15	11	20	35
Cr x	93.70	27.35	11.06	4.58	3.68	2.25	4.97	16.58	15.84
σ	72.42	16.77	8.55	3.47	5.40	2.00	2.21	17.34	15.58
Co x	31.82	14.37	7.56	2.51	2.47	3.25	2.73	6.59	7.01
σ	12.95	5.92	2.71	1.12	2.62	2.65	1.17	3.52	7.11
Ni x	33.90	9.25	5.78	3.44	3.11	3.49	5.85	7.20	8.37
σ	17.86	2.97	3.42	2.37	2.87	1.05	5.80	5.66	6.65
Cu x	27.18	11.16	15.97	7.60	4.89	9.37	24.11	15.87	18.69
σ	22.72	7.73	12.74	3.76	1.31	8.26	2.09	14.15	23.18
Zn x	72.31	2.74	24.03	12.78	10.24	7.06	13.92	17.31	17.34
σ	45.57	5.85	29.84	19.74	17.60	6.85	1.70	12.75	14.59
Nb x	8.63	9.98	6.36	4.41	1.66	1.53	3.11	3.32	9.29
σ	6.06	5.43	6.94	6.10	1.85	0.93	2.02	0.86	5.31
Ta x	0.44	0.61	0.45	0.29	0.11	0.09	0.28	0.17	0.81
σ	0.37	0.23	0.61	0.27	0.06	0.02	0.10	0.04	0.49
La x	23.75	35.44	44.37	15.24	5.73	10.63	17.20	17.34	47.07
σ	17.24	12.86	36.24	11.27	4.57	13.35	4.85	11.45	46.08
Ce x	50.80	68.26	81.54	28.07	10.66	20.76	32.41	32.42	87.9
σ	33.23	27.39	71.71	21.53	10.15	24.79	8.29	19.59	85.76
Pr x	6.50	8.31	9.91	2.84	1.27	2.20	3.95	3.61	9.73
σ	4.13	3.71	10.74	2.02	1.21	2.81	1.16	2.14	9.44
Nd x	25.66	28.13	34.78	8.86	4.79	7.68	13.41	12.63	34.88
σ	15.47	12.14	41.82	5.64	4.64	10.11	3.99	7.05	33.43
Sm x	5.13	4.58	5.49	1.23	0.97	1.41	2.44	2.10	4.95
σ	2.47	2.13	7.62	0.62	0.78	1.51	0.62	0.82	4.22
Eu x	1.33	1.29	1.44	0.67	0.78	0.83	0.81	0.78	1.27
σ	0.42	0.41	1.45	0.15	0.34	0.27	0.13	0.20	0.58
Gd x	4.80	3.98	4.05	0.88	0.65	0.91	1.43	1.70	4.25
σ	2.00	2.14	5.52	0.41	0.61	1.04	0.43	0.71	3.91

Table 7. (Contd.)

Element	*Sch* (7)	*Mig* (3)	Lc_1 (11)	Lc_2 (9)	Lc_3 (4)	Lc_4 (5)	Lc_5 (3)	Lc_6^{avt} (6)	Lc_6^{all} (3)
Tb x	0.69	0.50	0.50	0.10	0.09	0.13	0.15	0.22	0.51
σ	0.21	0.26	0.72	0.05	0.09	0.14	0.05	0.07	0.46
Dy x	3.97	2.35	2.25	0.40	0.37	0.51	0.53	1.04	2.35
σ	1.06	1.29	3.59	0.14	0.33	0.66	0.16	0.38	2.03
Ho x	0.78	0.41	0.37	0.07	0.07	0.09	0.09	0.20	0.38
σ	0.21	0.22	0.59	0.02	0.07	0.10	0.02	0.07	0.32
Er x	2.13	1.12	1.02	0.17	0.15	0.26	0.18	0.49	1.09
σ	0.49	0.58	1.77	0.08	0.15	0.25	0.03	0.21	0.90
Tm x	0.30	0.16	0.14	0.03	0.03	0.05	0.03	0.08	0.15
σ	0.08	0.09	0.21	0.01	0.02	0.04	0.01	0.03	0.11
Yb x	1.83	0.99	0.87	0.17	0.20	0.22	0.16	0.43	0.97
σ	0.56	0.59	1.58	0.06	0.20	0.23	0.04	0.17	0.74
Lu x	0.31	0.15	0.13	0.03	0.03	0.05	0.05	0.07	0.14
σ	0.09	0.09	0.20	0.01	0.02	0.05	0.002	0.02	0.09
Y x	21.46	12.02	10.35	1.74	1.87	2.50	2.234	5.36	11.40
σ	5.46	7.07	16.33	0.76	1.92	2.90	0.56	1.93	9.41
Zr x	154		244	114	65	60	104	104	129
σ	86		194	81	53	30	18	23	34
Hf ı	3.93		6.77	2.66	1.71	1.70	2.73	2.62	3.74
σ	1.96		5.91	1.36	1.12	0.84	0.82	0.51	1.02
Th x	3.35	5.98	8.60	2.99	0.65	2.89	2.60	3.06	12.92
σ	4.19	1.87	8.84	2.84	0.44	2.86	0.95	2.71	7.63
U x	0.79	0.87	0.62	0.34	0.21	0.24	0.50	0.52	1.66
σ	0.58	0.69	0.60	0.30	0.07	0.11	0.22	0.33	0.63
REE x	127.99	155.69	186.86	58.77	25.81	45.73	72.83	73.11	195.63
σ	75.57	63.55	179.89	41.39	22.98	55.17	19.52	43.40	188.00
LREE x	111.86	144.74	176.10	56.24	23.42	42.68	69.42	68.10	184.53
σ	72.20	58.04	165.73	40.79	21.32	52.52	18.70	40.99	178.85
HREE x	14.80	9.66	9.32	1.85	1.61	2.22	2.60	4.23	9.83
σ	3.95	5.24	14.14	0.70	1.50	2.50	0.70	1.53	8.76
$(La/Yb)_n$ x	9.62	27.32	73.33	67.58	22.38	32.33	75.99	27.62	29.14
σ	7.60	8.32	84.16	45.23	8.02	17.21	24.95	18.86	7.08
Eu/Eu* x	0.88	0.98	1.13	1.65	2.03	1.96	1.14	1.19	1.09
σ	0.15	0.17	0.31	0.59	0.66	0.68	0.13	0.13	0.47
Sm/Nd x	0.22	0.16	0.15	0.15	0.23	0.23	0.18	0.18	0.15
σ	0.05	0.01	0.02	0.04	0.05	0.06	0.02	0.04	0.02
Th/U x	4.05	9.94	13.99	9.87	3.43	8.19	5.41	5.09	7.39
σ	2.79	7.90	11.07	9.59	0.82	7.08	0.85	1.78	1.97
K/Rb x	382	270	409	528	630	444	590	441	424
σ	146	44	131	274	80	68	164	201	57
Rb/Ba x	0.098	0.093	0.059	0.029	0.022	0.032	0.027	0.043	0.047
σ	0.054	0.026	0.035	0.01	0.011	0.021	0.013	0.019	0.015
Rb/Sr x	0.063	0.119	0.057	0.047	0.064	0.054	0.012	0.042	0.098
σ	0.036	0.096	0.027	0.031	0.026	0.025	0.009	0.014	0.033

Note: Numerals in parentheses correspond to the number of samples; x is the average, σ is the standard deviation.

do not exhibit any systematic changes in their concentrations in the leucosomes (Table 8). The comparison of the series $\longrightarrow Lc_2$, Lc_3, Lc_4 and $Lc_6^{avt} \longrightarrow Lc_6^{all}$ also reveals different signs of the changes in the concentrations of LREE, HREE, Eu, Zr, Hf, Th, U, Y, Nb, Ta, and Cs: these concentrations decrease in the former series and increase in the latter. At the same signs of the changes in the concentrations, the decrease in the V, Cr, Co, Ni, Sc, and Li concentrations and the increase in the Rb, Ba, and Pb concentrations are more significant in the former series.

Below we will consider only correlations between the concentrations of elements in the rock groups that can be interpreted. The sum of the TiO_2, MgO, and FeO* contents, which indicates how mafic (*maf*) a rock is, tends to be positively correlated with the sum of the concentrations of such elements as V, Cr, Ni, and Co, and the regression lines are individual for each of the groups (Table 9, Fig. 11). An analogous character is typical of the correlations between *maf* and the HREE, Zr, and Hf concentrations in the joint sampling Lc_2 + Lc_4. This is most probably explained by the fact that the vein leucosomes contain zircon mostly included in biotite or, more rarely, in garnet and hornblende, while this mineral in other rock groups occurs mostly at grain boundaries. Analogous relations were also discovered in other migmatite complexes (Glebovitsky and Sedova, 1998). A positive correlation between P_2O_5 and LREE is displayed by almost all of the groups and testifies that LREE strongly enrich apatite. It is worth noting that a weak positive correlation between LREE and Si is typical of the basic rocks and becomes negative in the leucosomes: it is statistically insignificant in Lc_1 but becomes significant in Lc_2, Lc_3, Lc_4, and Lc_6^{all}, i.e., in anatectic varieties. As usual, positive correlations are shown by K with Rb (Fig. 11) and Ba, without significant differences in the K/Rb and K/Ba ratios but with a tendency toward a decrease in the K/Rb ratio in Lc_4 and an increase in K/Ba in the basites (Table 7). Noteworthy positive correlations are displayed by K–LREE and K–HREE in Lc_1 and by K–LREE in Lc_2, which are absent from other groups (Table 9). The aforementioned anomalously high LREE concentrations in Lc_1 are typical of the most potassic varieties. This is the only group exhibiting positive correlations between K and Y, Zr, Hf, Nb, Ta, Th, and U. In contrast to intrusive granitoid complexes (Sedova et al., 2004), the leucosomes show no correlations of their Sr and Eu concentrations with either the content of normative plagioclase or the anorthite concentration in the latter. Positively sloped LREE–HREE, La–Yb, and Sm–Nd trends were revealed in all of the compared rock groups, except *Sch*, Lc_2, and Lc_6^{avt} (Fig. 11). Positive Y-HREE, U–Th, and Th–LREE correlations persist in all of the groups (Table 9).

DISCUSSION AND CONCLUSIONS

The data presented above on the geology, petrology, and geochemistry of granite-gneisses and migmatites that development after rocks of the El'gakan unit led us to certain conclusions concerning the evolution of the rock compositions in the process of their granitization and migmatization, and the data obtained on zircons make it possible to date these processes.

The protoliths of the early ultrametamorphic products consisted of an association of magmatic rocks corresponding to the calc–alkaline series with a pronounced subalkaline trend (trachybasalts, trachybasaltic andesites, and sometimes, shoshonites). Judging from the occurrence of melt inclusions with glass in the early zircon populations, a significant role in this series was played by volcanic rocks (Glebovitsky et al., 2007).

Granitization processes are geochemically notably different from migmatization processes, in which a significant part was played by melting. This is most vividly manifested in the behavior of LREE, Zr, Hf, and Th, which enrich during early granitization, while migmatization series show systematic depletion in these elements (Tables 7, 8). In both processes, the rocks are depleted in such incompatible and transition elements as V, Cr, Co, Ni, and Sc, but the removal of these elements during granitization is more active. Migmatization processes of different age also differ geochemically. The series protolith $\longrightarrow Lc_2$, Lc_3, and Lc_4 and $Lc_6^{avt} \longrightarrow Lc_6^{all}$ display different signs of the changes in the concentrations of LREE, HREE, Eu, Zr, Hf, Th, U, Y, Nb, Ta, and Cs: the concentrations of these elements decrease in the former series and increase in the latter. At the same time, the decrease in the contents of V, Cr, Co, Ni, Sc, and Li and the increase in the concentrations of Rb, Ba, and Pb are more significant in the former series. The behavior of Nb and Ta deserves special consideration: these elements show a persistent tendency toward depletion during granitization and early migmatization. At the same time, strong melt fractionation during the origin of granites Lc_6^{all} is associated with enrichment in these elements.

Correlations established between elements in the rock groups are controlled by the geochemical similarities between the elements (for example, K–Rb, K–Ba, Sm–Nd, Th–LREE, and Y–HREE; Table 9). Certain differences were revealed in the character of correlations between elements in the rock groups due either to the setting of zircons in these rocks (at grain boundaries or as inclusions in mafic minerals) or the character of the predominant granite-forming processes. In the process of the volume replacement of basite by granite-gneiss (Lc_1), the latter acquire new correlation features: Ta–HREE, Ta–LREE, Nb–LREE, Zr–HREE, Zr–Yb, Zr–Y, K–HREE, and K–LREE, which are absent in the basites (Table 9). These correlations later disappear during the partial melting that produced leucosomes

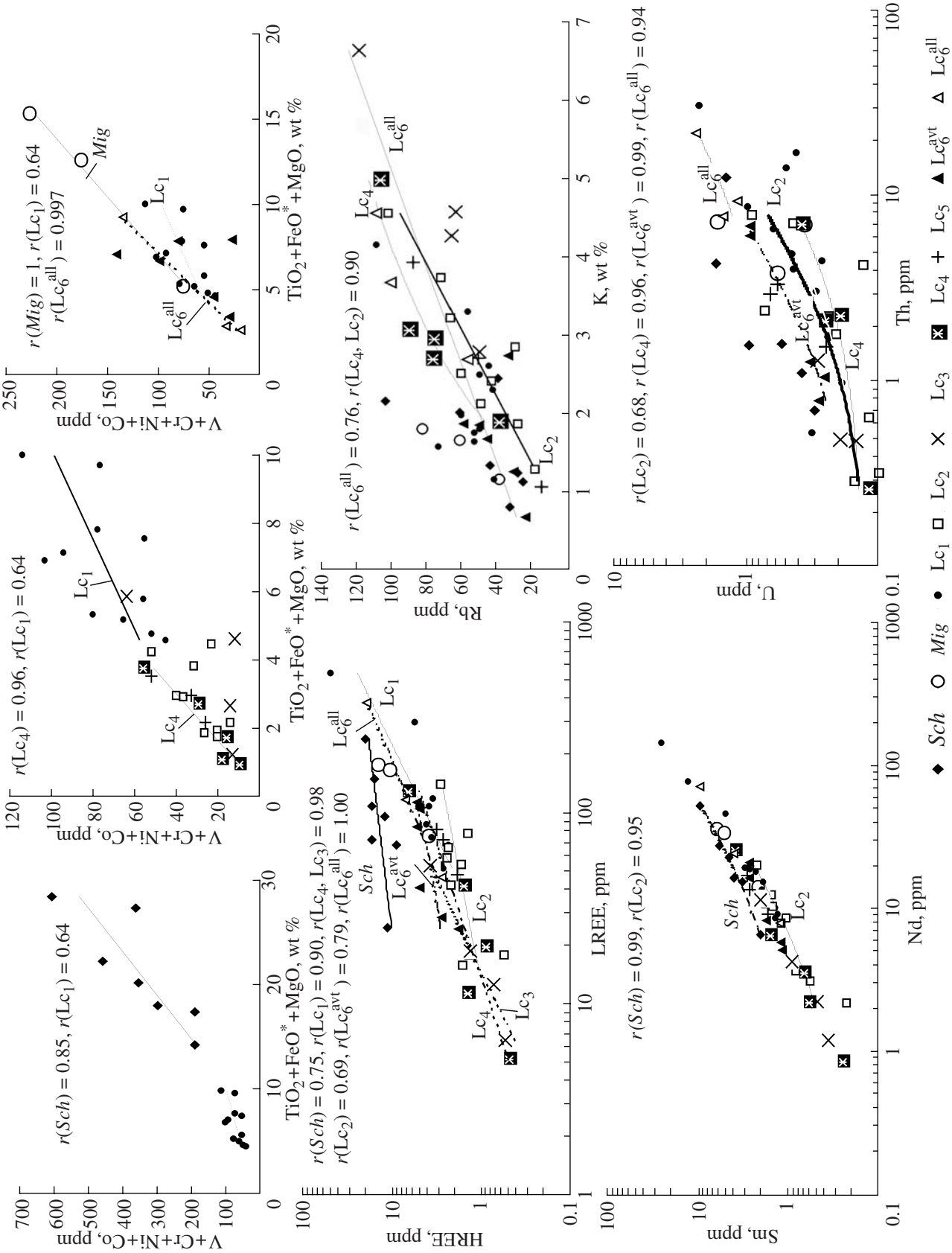

Fig. 11. Diagrams (V + Cr + Ni + Co)–(TiO_2 + FeO*+MgO), HREE–LREE, Rb–K, Sm–Nd, and U–Th for the rocks. See Fig. 9 for the abbreviations of the rock groups. The diagrams show statistically significant values of *r* and trends.

Table 8. Average ratios of elements in products of ultrametamorphism and protolithic rocks and trends in the rock transformations during ultrametamorphism

	V	Cr	Co	Ni	Sc	Li	Be	Cs	Rb	Sr	Ba	Pb	LREE	Eu	HREE	Zr	Hf	Th	U	Y	Nb	Ta
Lc_1/Sch, x	0.28	0.22	0.26	0.19	0.18	0.95	0.78	1.30	1.35	1.77	2.67	1.36	2.33	1.1	0.63	1.84	1.97	6.65	1.18	0.48	0.71	0.75
σ	0.15	0.19	0.18	0.14	0.18	0.19	0.37	1.11	0.44	0.98	2.22	0.55	1.79	0.83	0.86	1.24	1.45	7.74	1.18	0.75	0.75	1.13
N_1, <1	11	11	11	11	11	6	7	5	3	1	1	4	3	6	10	2	3	4	6	10	10	10
N_2, >1						5	4	6	8	10	10	5	8	5	1	9	8	7	5	1	1	1
Lc_2/Lc_1 x	0.41	1.06	0.32	0.60	0.62	1.8	1.17	0.68	0.89	0.99	1.60	1.02	0.46	0.69	0.40	0.54	0.52	0.56	0.86	0.35	1.10	1.69
σ	0.12	7	0.19	0.28	0.88	2.34	0.76	0.40	0.58	0.39	1.25	0.41	0.35	0.36	0.23	0.28	0.34	0.56	0.88	0.23	1.77	2.81
N_1, <1	9	2	9	8	8	3	5	8	6	4	3	4	8	7	9	9	7	8	6	9	8	2
N_2, >1				1	1	6	4	1	3	5	6	5	1	2			2	1	3		1	7
$Lc_3/Lc_1 + Mig$ x	0.34	0.88	0.34	0.75	0.18	0.30	1.26	0.56	1.42	2.55	12.1	1.24	0.17	0.67	0.23	0.27	0.17	0.11	0.30	0.24	0.26	0.38
σ	0.29	1.68	0.38	0.89	0.26	0.27	0.89	0.40	0.50	2.98	14.1	0.77	0.22	0.58	0.31			0.11	0.18	0.31	0.34	0.37
N_1, <1	8	7	7	6	8	8	4	6	2			3	8	6	8	6	6	8	8	8	7	7
N_2, >1		1	1	2			4	2	6	8	8	5		2							1	1
$Lc_4/(Lc_1 + Mig)$ x	0.32	0.34	0.33	0.49	0.25	0.31	1.23	0.82	1.66	1.50	8.55	1.51	0.50	1.00	0.54	0.38	0.43	1.43	0.75	0.52	0.51	2.74
σ	0.21	0.47	0.25	0.22	0.41	0.17	0.99	0.56	0.48	1.10	10.8	0.69	0.84	0.55	0.77			2.59	0.66	0.68	0.48	3.88
N_1, <1	7	6	7	7	6	7	3	5	1	1	1	2	6	3	6	6	6	5	5	6	6	5
N_2, >1		1			1		4	2	6	6	6	5	1	4	1			2	2	1	1	2
$Lc_6^{avt}/(Lc_1 + Mig + Sch)$ x	0.55	0.37	0.49	0.55	0.71	0.50	1.20	0.56	0.69	1.48	1.63	0.92	0.67	0.76	0.73	0.55	0.70	0.91	0.87	0.75	0.72	0.83
σ	0.11	0.39	0.14	0.32	0.23	0.16	0.67	0.25	0.14	1.11	1.36	0.17	0.47	0.34	0.55	0.15	0.40	0.76	0.55	0.56	0.59	0.65
N_1, <1	6	5	6	5	5	6	4	6	6	3	2	4	5	5	5	3	2	5	5	5	5	4
N_2, >1		1		1	1		2			3	4	2	1	1	1		1	1	1	1	1	2
Lc_6^{all} / Lc_6^{avt} x	0.63	0.75	0.81	0.69	0.56	0.89	1.48	1.41	2.25	0.87	1.92	1.77	3.00	1.43	1.80	1.47	1.60	6.74	3.88	1.67	2.60	4.65
σ	0.49	0.66	0.61	0.32	0.75	0.35	0.33	0.53	0.56	0.28	0.80	0.32	4.21	0.78	1.45	0.45	0.76	9.25	3.62	1.00	1.17	2.22
N_1, <1	3	2	3	3	3	2				3			1	1	1					1	1	
N_2, >1	1	2	1	1	1	2	4	4	4	1	4	4	3	3	3	3	3	4	4	3	3	4

Note: x is the average, σ is the standard deviation, N_1 and N_2 are the numbers of series in which a decrease (<1) or increase (>1) of the concentration of a given element was detected in the ultrametamorphic products relative to those in the protolithic rocks. In the analyzed series, the protolith of Lc_1 consisted of crystalline schists *Sch*; the protolith of Lc_2 was Lc_1; the protolith of Lc_3 and Lc_4 was Lc_1 and migmatites *Mig*; the protoliths of Lc_6^{avt} were Lc_1, migmatites *Mig*, and crystalline schists *Sch*; the protolith of Lc_6^{all} –Lc_6^{avt}.

Table 9. Pair correlation coefficients (r) of some elements in rock groups in the ultrametamorphic zone in the middle and lower reaches of the Nyukzha River

Correlated elements	*Sch*	Lc_1	Lc_2	Lc_3	Lc_4	$Lc_2 + Lc_4$	Lc_5	Lc_6^{avt}	Lc_6^{all}
	Number of samples								
	7	11	9	4	5	14	3	6	3
	$r_{0.05}$								
	0.754	**0.602**	**0.666**	**0.950**	**0.878**	**0.532**	**0.997**	**0.811**	**0.997**
Maf–CoNiCrV	**0.846**	**0.638**	0.575	0.732	**0.950**	**0.719**	0.929	0.417	**0.997**
Maf–HREE	0.034	0.197	0.417	0.840	0.858	**0.532**	0.303	0.481	0.973
Maf–Zr	–0.500	0.577	0.053	**0.964**	0.704	0.253		**–0.839**	0.270
Maf–Hf	–0.477	0.370	0.467	**0.950**	0.817	**0.594**		–0.700	0.140
P_2O_5–LREE	0.740	**0.720**	**0.697**	0.752	**0.967**	**0.820**	0.884	0.720	0.950
SiO_2–LREE	0.503	–0.400	**–0.805**	–0.899	**–0.875**	**–0.745**	0.125	–0.271	–0.986
SiO_2–HREE	–0.040	–0.500	–0.526	–0.870	–0.828	**–0.818**	–0.297	–0.071	–0.974
K–Rb	0.600	**0.627**	**0.899**	**0.955**	**0.897**	**0.868**	**0.995**	0.400	0.943
K–Ba	0.715	**0.927**	**0.789**	0.872	0.023	0.130	**0.942**	**0.871**	0.077
K–LREE	0.544	**0.691**	0.661	–0.091	0.180	0.397	0.764	0.610	–0.767
K–HREE	0.504	**0.623**	0.385	–0.140	0.095	0.177	0.655	0.510	–0.729
LREE–HREE	0.745	**0.898**	**0.696**	**0.997**	**0.980**	**0.770**	0.988	0.790	0.998
La–Yb	–0.153	**0.719**	0.217	**0.983**	**0.928**	**0.553**	0.548	0.470	0.996
Sm–Nd	**0.993**	**0.993**	**0.947**	**0.998**	**0.990**	**0.952**	0.932	**0.971**	0.995
Y–HREE	**0.914**	**0.999**	**0.858**	**0.999**	**0.999**	**0.977**	0.990	**0.900**	**0.998**
U–Th	0.674	**0.841**	**0.683**	0.937	**0.958**	**0.687**	0.934	**0.991**	0.940
Ta–Nb	**0.924**	**0.918**	0.300	0.810	0.451	0.367	0.971	0.583	**0.998**
Ta–HREE	0.247	**0.760**	–0.060	0.752	0.231	–0.050	0.982	0.588	0.800
Ta–LREE	–0.236	**0.818**	–0.450	0.749	0.213	–0.249	0.942	0.026	0.765
Nb–HREE	0.464	**0.943**	–0.639	**0.991**	0.772	–0.185	**0.999**	0.752	0.764
Nb–LREE	0.063	**0.919**	–0.436	**0.995**	0.850	–0.201	0.995	0.645	0.726
Zr–HREE	0.324	**0.981**	0.455	**0.997**	0.538	0.150		0.235	0.482
Zr–Yb	–0.437	**0.848**	0.614	**0.999**	0.562	0.189		0.343	0.766
Zr–Y	0.119	**0.902**	0.609	**0.997**	0.525	0.173		0.347	0.537
Th–LREE	**0.858**	**0.616**	**0.699**	**0.993**	**0.976**	**0.882**	0.888	**0.920**	0.955

Note: Maf is maficity, which is equal to the sum of concentrations of TiO_2 + MgO + FeO*; LREE and HREE are the concentrations of light and heavy REE (without Eu. Printed in bold are statistically significant (at a significance level of 0.05) correlation coefficients, $r_{0.05}$ is the correlation coefficient significant at a given number of samples in each group.

Lc_2 and Lc_4 and are partly inherited by leucosomes Lc_3, which were generated by diatexis (in contrast to the genesis of other groups of leucosomes). Note that Lc_6^{avt} show much less correlations than Lc_1 do, which may be explained by the instable, uncompleted, brief duration, and local character of the volume replacement process, which proceeded concurrently with melting and rheomorphism. Moreover, the two rock groups were derived from different protoliths: Lc_6^{avt} developed after Lc_1 with relics of basic rocks and after migmatites with leucosomes Lc_2, Lc_3, and Lc_4, whereas Lc_1 were derived in our case exclusively from basites *Sch*.

Not going into much detail of the results of our geochemical simulations, we only mention that, for leucosomes whose protoliths are known, consistency can practically always be achieved between the REE concentrations (mostly LREE) in the rocks and those

calculated for the melt by the model of equilibrium melting (Allegre and Minster, 1978; Prinzhofer and Allegre, 1985; Sawyer, 1991). The inconsistencies for HREE are explained by the occurrence of allanite, sphene, and magnetite in some of the samples (these elements were not taken into account in the simulations). Data on the composition of individual zircon populations demonstrate that the fraction of LREE contained in various zircon types is insignificant in both Lc_1 (0.02–0.002 wt %) and Lc_5 (0.02–0.03 wt %). The HREE distribution is different: much of these elements (8 wt %) is contained in Lc_1 in zircons of phases I, II, and III and only little of them (0.4 wt %) is contained in zircon of phase IV. The fraction of HREE in Lc_5 in both of the types is insignificant but is more appreciable in the early one (19 and 6 wt %). All of these facts testify that the results of the HREE simulations should be regarded as qualitative but not quantitative. Note that some trace elements (Zr, Hf, Th, Y, Ta, and Nb) behave similarly to either LREE or HREE. An independent behavior is commonly displayed by elements geochemically similar to K: Rb, Cs, Ba, and Sr. The increase in the Rb concentration in the leucosomes of the migmatites at a decrease in the LREE contents can be explained by the introduction of the former element, although in some instances (for example, when Lc_5 are produced), this can be explained by melt fractionation.

It is now pertinent to discuss our results obtained on the zircons. The age of zircons of phase I, which contain melt inclusions with glass, from Lc_1 (3010 Ma) corresponds to the age of the protolith of the plagiogneisses (mafic volcanics). Judging by the occurrence of inclusions of recrystallized melts, CO_2, and acicular apatite (Glebovitsky et al., 2007), zircons of phases II and III (2703 Ma) crystallized at the peak of metamorphism and ultrametamorphism, which corresponded to the granulite facies in our study area, whereas type IV of the zircons (1915 Ma), which is the most widely spread in the rocks, was likely formed during an overprinted metamorphic process, whose temperature and pressure did not exceed the peak conditions of the early metamorphism. The REE patterns also testify that the crystallization conditions of individual zircon types have changed. The decrease in the HREE concentrations (Fig. 5) in zircons of types III and, particularly, IV (in contrast to types II and III) suggests that the garnet may have crystallized simultaneously with or earlier than the zircon, which finds further support in the occurrence of garnet inclusions in the zircons of types III and IV. A decrease in the REE concentration and the Th/U ratio in the zircon rims relative to their cores is thought to be explained by the effect of various processes: overprinted metamorphism or anatectic melting (Varta et al., 1999; Zeck and Whitehouse, 1999; Rubatto et al., 2001; Skublov, 2005). The zircons of type III are characterized by REE patterns typical of granitoids and the leucosomes of migmatites (Belousova et al., 2002) but differ from them in having high Th/U ratios (Table 2, Fig. 4). This likely provides evidence of some unusual crystallization conditions of zircons of this type, for example, a high oxygen fugacity, at which sexavalent U is retained in the fluid (or in the melt). Zircon rims from Lc_6^{avt}, show genetic features close to those of zircons of type III from Lc_1 and also have high Th/U ratios (>1; Table 4, Fig. 4). Zircon rims from Lc_5 are characterized by higher Th/U ratios than those of type-III zircons from Lc_1 and zircon margins from Lc_6^{avt}, and approach in this sense type-IV zircons (Lc_1). These zircons have REE concentrations intermediate between those in zircons of types III and IV but have, like the latter, Eu and Ce anomalies (Figs. 4, 5). These features are typical of zircons of metamorphic genesis, which crystallize in the absence of melt (Hoskin and Schalteger, 2003; Rubatto et al., 2001; Rubatto, 2002). This does not pertain to Lc_5, and it is unreasonable to assume that the zircons were modified during the late magmatic stage. The analyzed rims of rhythmically zonal zircon most probably grew early in the process of garnet crystallization, before the onset of fractional crystallization, during which zircons became enriched in REE, U, and Th (Belousova et al., 2006).

Our zircon dates are in good agreement with earlier results obtained on granulite complexes in the Dzhugdzhur–Stanovoi foldbelt. The age of the magmatic protolith of rocks of the El'gakan unit is close to 3 Ga and indicates that these rocks are the oldest in the territory in question. This is consistent with the age estimates of the major metamorphic stages and with data on the Nd systematics, which provide evidence of ancient continental crustal growth at 2.9–3.1 Ga (Kotov et al., 1999). The oldest metamorphism in the region (2812 ± 1 Ma) was identified in studying charnockites of the Kurul'ta block (Sal'nikova et al., 2004b). Metamorphism at 2703 Ma, to which, reportedly, the granitization of the El'gakan unit was related, was proved to be synchronous with granulite-facies metamorphism (widespread in the territory) at 2647–2718 Ma: at 2647 ± 3 Ma in the Dambukta block (Larin et al., 2004), 2718 ± 20 Ma in the Kurul'ta block (Sal'nikova et al., 2004b), and 2650 Ma in the Larba block (Bibikova et al., 1984). The latter date was obtained on a zircon inclusion in garnet from a granulite mineral assemblage, which does not rule out a younger age of the metamorphism. The age of the granulite metamorphism is slightly older than the age when the anorthosites of the Kalar Massif were emplaced (2638 ± 36 Ma) and then metamorphosed (2623 ± 20 Ma) (Sal'nikova et al., 2004a; Larin et al., 2004, 2006a). Note that this process occurred in the territory in question under amphibolite-facies conditions, which indicates that the Archean metamorphism was heterogeneous.

The most widely spread zircons of type IV from granite-gneisses have a concordant age of 1915 Ma, which is in good enough agreement with recent data on the age of granulite metamorphism in the Dzhugdzhur–

Stanovoi foldbelt. This metamorphic event can be easily traced throughout the whole Fore-Stanovoi belt, was identified in the Dambukta (Kotov et al., 1999; Larin et al., 2004; Sal'nikova et al., 2004a, 2004b), Larba, and Mogocha (Gavrikova et al., 1991) blocks, and accompanied collision between the Dzhugdzhur–Stanovoi foldbelt and Siberian craton. These collision processes manifested themselves in the El'gakan unit as the development of the imbricated nappe structures, but the overprinted metamorphism itself occurred there under conditions of the amphibolite and epidote-amphibolite facies and was likely related to the origin of the Dzheltulak Complex (Sudovikov et al., 1965).

Granites Lc_5 are geologically comparable with the Late Stanovoi granites and were proved to be coeval with them (zircon dating). The most important issue is that these granites were proved simultaneous with the migmatites that developed after the Ilikan unit of the Stanovoi Complex (Larin et al., 2006b). This suggests that deep-seated zones are exposed in the western Dzhugdzhur–Stanovoi foldbelt, where crustal granite magmas were generated in the Mesozoic, as also follows from data on migmatites Lc_6.

ACKNOWLEDGMENTS

This study was supported by the Russian Foundation for Basic Research (project nos. 05-05-65128, 04-05-64156) and a grant from the President of the Russian Federation (Grant NSH-4732.2005.5).

REFERENCES

1. G. J. Allegre and J. F. Minster, "Quantitative Models of Trace Element Behavior in Magmatic Processes," Earth Planet. Sci. Lett. **38**, 1–25 (1978).
2. E. A. Belousova, W. F. Griffin, and S. Y. O'Reily, "Igneous Zircon: Trace Element Composition as an Indicator of Source Rock Type," Contrib. Mineral. Petrol. **143**, 602–622 (2002).
3. E. A. Belousova, W. F. Griffin, and S. Y. O'Reily, "Zircon Crystal Morphology, Trace Element Signatures and Hf Isotope Composition as a Tool for Petrogenetic Modeling: Examples from Eastern Australian Granitoids," J. Petrol. **47**, 329–353 (2006).
4. E. V. Bibikova, V. I. Shul'diner, T. V. Gracheva, et al., "Isotopic Age of Granulites in the Western Stanovoy Area," Dokl. Akad. Nauk SSSR **275** (6), 1471–1474 (1984).
5. W. V. Boynton, "Cosmochemistry of the Rare Earth Elements Meteorite Studies," in *Rare Earth Element Geochemistry* (Elsevier, Amsterdam, 1984), pp. 63–114.
6. S. V. Efremova and K. G. Stafeev, *Petrochemical Methods in Studying Rocks* (Nauka, Moscow, 1985) [in Russian].
7. S. N. Gavrikova and V. A. Zharikov, "Geochemical Features of the Granitization of Archean Rocks in Eastern Transbaikalia," Geokhimiya, No. 1, 26–49 (1984).
8. S. N. Gavrikova, L. L. Nikolaeva, A. V. Galanin, et al., *Early Precambrian of the Southern Part of the Stanovoy Fold Province* (Nedra, Moscow, 1991) [in Russian].
9. V. A. Glebovitskii and I. S. Sedova, "Anatexis and Formation of Crustal Magmatic Chambers: Petrological and Geological Evidence (Belomorian and Svecofennican Provinces, Baltic Shield)," Zap. Vseross. Mineral. O-va, No. 4, 5–26 (1998).
10. V. A. Glebovitskii and I. S. Sedova, "Amphibolite-Facies Ultrametamorphism of the Stanovoy Complex," Dokl. Akad. Nauk SSSR **279** (2), 434–437 (1984).
11. V. A. Glebovitsky, I. S. Sedova, D. I. Matukov, et al., "Age of the Stanovoy Complex of East Siberia: Evidence from SHRIMP II Ion Microprobe Data," Dokl. Akad. Nauk **412** (3), 365–368 (2007) [Dokl. Earth Sci. **412**, 29–34 (2007)].
12. V. A. Glebovitskii, I. S. Sedova, and L. M. Samorukova, "Peculiarities in the Behavior of Trace and Rare Earth Elements during Granitization and Migmatization of the Elgakan Complex (East Siberia, Nyukzha River)," Dokl. Akad. Nauk **411** (2), 231–234 (2006) [Dokl. Earth Sci. **411**, 1303–1308 (2006)].
13. P. W. O. Hoskin and U. Schaltegger, "Composition of Zircon and Igneous and Metamorphic Petrogenesis," Rev. Mineral. Geochem. **53**, 27–62 (2003).
14. V. M. Kastrykina, "Metamorphism of the Central Part of the Dzhugdzhur–Stanovoy Fold Area," in *Precambrian Metamorphism of the Baikal–Amur Railway Area* (Nauka, Leningrad, 1983), pp. 140–163 [in Russian].
15. *Classification and Nomenclature of Magmatic Rocks*, Ed. by O. A. Bogatikov, N. P. Mikhailov, and V. I. Gon'shakova (Nedra, Moscow, 1981) [in Russian].
16. D. S. Korzhinskii, "Precambrian of the Aldan Plate and Stanovoi Range," in *Stratigraphy of USSR* (Akad. Nauk SSSR, Moscow–Leningrad, 1939), Vol. 1, pp. 349–366 [in Russian].
17. A. B. Kotov, V. M. Shemyakin, E. B. Sal'nikova, and V. P. Kovach, "Formation Stages and Isotope Structure of the Continental Crust of the Sutam Block, Aldan Shield: Evidence from Sm–Nd Isotope Systematics of Granitoids," Dokl. Akad. Nauk **366** (6), 809–812 (1999) [Dokl. Earth Sci. **367**, 695–697 (1999)].
18. A. M. Larin, A. B. Kotov, E. B. Sal'nikova, et al., "The Kalar Complex, Aldan Stanovoi Shield, an Ancient Anorthosite–Mangerite–Charnockite–Granite Association: Geochronologic, Geochemical, and Isotopic-Geochemical Characteristics," Petrologiya **14** (1), 4–24 (2006b) [Petrology **14**, 2–20 (2006b)].
19. A. M. Larin, A. B. Kotov, E. B. Sal'nikova, et al., "Mesozoic Granites of the Chubachin Massif, Tukuringra Complex, Dzhugdzhur–Stanovoi Foldbelt: New Geochemical, Geochronological, and Isotopic-Geochemical Evidence," Petrologiya **9** (4), 417–432 (2001) [Petrology **9**, 362–375 (2001)].
20. A. M. Larin, A. B. Kotov, E. B. Sal'nikova, et al., "New Data on the Age of Granites of the Kodar and Tukuringra Complexes, Eastern Siberia: Geodynamic Constraints," Petrologiya **8** (3), 267–279 (2000b) [Petrology **8**, 238–248 (2000b)].
21. A. M. Larin, A. B. Kotov, V. P. Kovach, et al., "Stages of Continental Crustal Formation in the Central Part of the Dzhugdzhur–Stanovoy Fold Area: Sm–Nd Isotopic Data

on Granitoids," in *Petrography on the Turn of 21th Century. Results and Prospects. Proceedings of 2nd All-Russian Petrographic Conference, Syktyvkar, 2000* (Syktyvkar, 2000a), pp. 61–62 [in Russian].

22. A. M. Larin, E. B. Sal'nikova, A. B. Kotov, et al., "Late Archean Granitoids of the Dambukinski Block of the Dzhugdzhur–Stanovoy Fold Belt: Formation and Transformation of the Continental Crust in the Early Precambrian," Petrologiya **12** (3), 1–19 (2004) [Petrology **12**, 211–226 (2004)].
23. A. M. Larin, E. B. Sal'nikova, A. B. Kotov, et al., "Early Cretaceous Age of Regional Metamorphism of the Stanovoi Group in the Dzhugdzhur–Stanovoi Foldbelt: Geodynamic Implications," Dokl. Akad. Nauk **409** (2), 222–226 (2006b) [Dokl. Earth Sci. **409**, 727–731 (2006b)].
24. N. I. Moskovchenko, G. V. Ovchinnikova, and V. M. Kastrykina, "High-Pressure Granulites of East Siberia in Terms of Archaean and Proterozoic Evolution," Precambrian Res. **62**, 473–491 (1993).
25. N. I. Moskovchenko, A. P. Semenov, and V. N. Verkhalo-Uzkii, "Granulite Complexes of the Stanovoy Fold Area," in *Early Precambrian of the Aldan massif and Its Framing* (Nauka, Leningrad, 1985), pp. 121–144 [in Russian].
26. A. Prinzhofer and G. J. Allegre, "Residual Peridotites and the Mechanism of Partial Melting," Earth Planet. Sci. Lett. **74**, 251–265 (1985).
27. D. Rubatto, "Zircon Trace Element Geochemistry: Partitioning with Garnet and the Link between U–Pb Ages and Metamorphism," Chem. Geol. **184**, 123–138 (2002).
28. D. Rubatto, I. S. Williams, and I. S. Buick, "Zircon and Monazite Response to Prograde Metamorphism in the Reynolds Range, Central Australia," Contrib. Mineral. Petrol. **140**, 458–468 (2001).
29. E. B. Sal'nikova, A. M. Larin, A. B. Kotov, et al., "The Kalar Anorthosite-Charnockite Complex of the Aldan–Stanovoi Shield: Age and Tectonic Implications," Stratigr. Geol. Korrelyatsiya **12** (3), 3–11 (2004a) [Stratigr. Geol. Correlation **12**, 221–228 (2004a)].
30. E. B. Sal'nikova, V. A. Glebovitskii, A. B. Kotov, et al., "Metamorphic Evolution of Granulites from the Kurul'ta Block, Aldan Shield: U–Pb Single Zircon Study," Dokl. Akad. Nauk **398** (2), 239–243 (2004b) [Dokl. Earth Sci. **398**, 968–972 (2004b)].
31. E. W. Sawyer, "Disequilibrium Melting and the Rate of Melt–Residium Separation during Migmatization of Mafic Rocks from the Greenville Front, Quebec," J. Petrol. **32**, 701–738 (1991).
32. I. S. Sedova and V. A. Glebovitsky, "Granite Formation under Amphibolite-Facies Conditions in the Stanovoy Complex," in *Early Precambrian of the Aldan Massif and its Framing* (Nauka, Leningrad, 1985), pp. 92–121 [in Russian].
33. I. S. Sedova and V. A. Glebovitsky, "Evolution Paths of Ultrametamorphism under Amphibolite-Facies Conditions," Izv. Akad. Nauk SSSR, Ser. Geol., No. 2, 46–60 (1984).
34. I. S. Sedova and V. A. Glebovitskii, "Ultrametamorhism and Granite Formation," in *Evolution of the Early Archean Lithosphere of the Aldan–Olekma–Stanovoy Region* (Nauka, Leningrad, 1987), pp. 200–224 [in Russian].
35. I. S. Sedova, L. M. Samorukova, V. A. Glebovitskii, and D. P. Krylov, " Geochemistry of Granitoids of the Svecofennian Tectonometamorphic Cycle in the Northern Ladoga Region," Petrologiya **12** (4), 394–414 (2004) [Petrology **12**, 348–366 (2004)].
36. V. I. Shul'diner, I. V. Panchenko, and I. S. Shul'diner, "Petrology of Metamorphic Complexes in the Nyukzha River Basin," in *Precambrian Metamorphism in the Baikal–Amur Railway Area* (Nauka, Leningrad, 1983), pp. 66–75 [in Russian].
37. S. G. Skublov, *Geochemistry of Rare-Earth Elements in Rock-Forming Metamorphic Minerals* (Nauka, St. Petersburg, 2005) [in Russian].
38. N. G. Sudovikov, V. A. Glebovitskii, G. M. Drugova, et al., *Geology and Petrology of the Southern Framing of the Aldan Shield* (Nauka, Leningrad, 1965) [in Russian].
39. G. Varva, R. Schmidt, and D. Gebauer, "Internal Morphology, Habit and U–Th–Pb Microanalysis of Amphibolite-to-Granulite Facies Zircons: Geochronology of the Ivrea Zone (Southern Alps)," Contrib. Mineral. Petrol. **134**, 380–404 (1999).
40. E. B. Watson and T. M. Harrison, "Zircon Saturation Revisited: Temperature Compositional Effects in a Variety of Crustal Magma Types," Earth Planet. Sci. Lett. **64**, 295–304 (1983).
41. H. P. Zeck and M. J. Whitehouse, "Herzian, Pan-African, Proterozoic and Archean Ion-Microprobe Zircon Ages for a Betic-Rif Core Complex, Alpine belt, W Mediterranean—Consequences for its *P–T–t* Path," Contrib. Mineral. Petrol. **134**, 134–149 (1999).
42. V. A. Zharikov and L. I. Khodorevskaya, "Generation of Granites after Amphibolites," Petrologiya **14** (4), 339–357 (2006) [Petrology **14**, 319–336 (2006)].